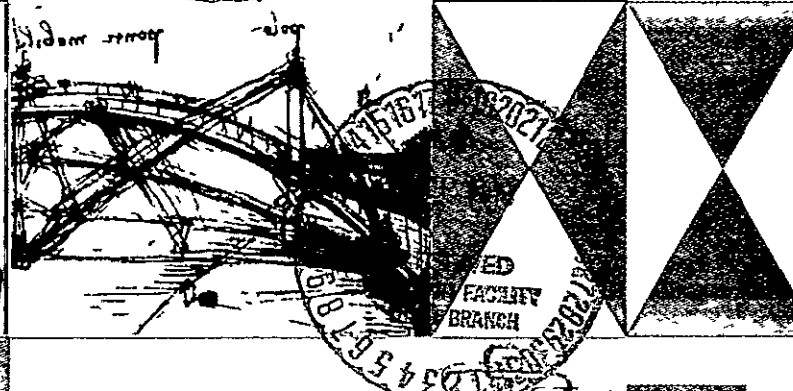
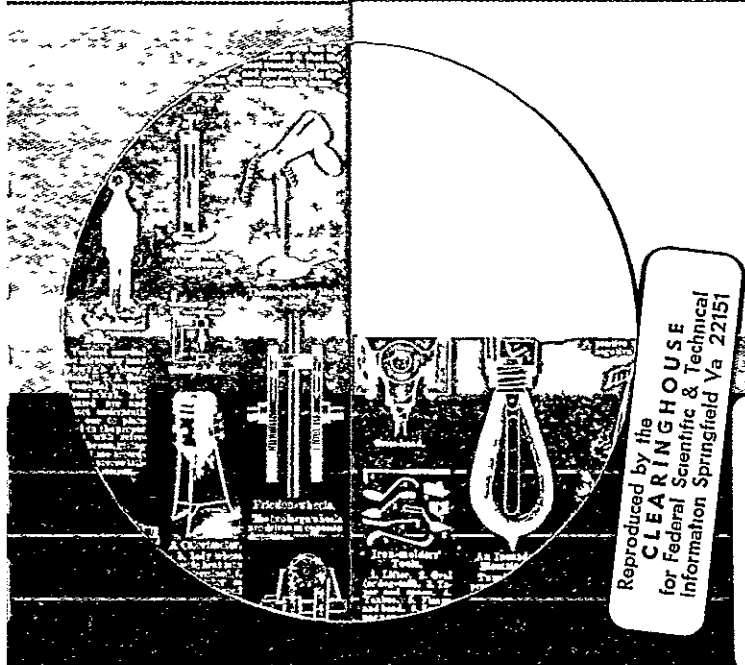
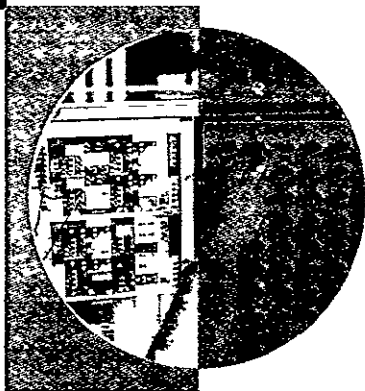
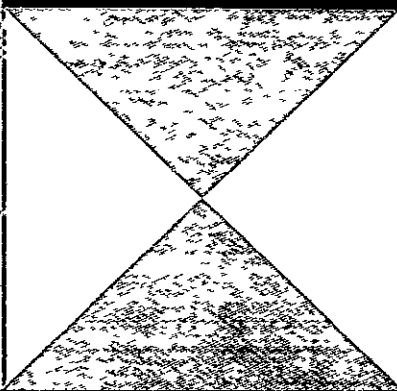
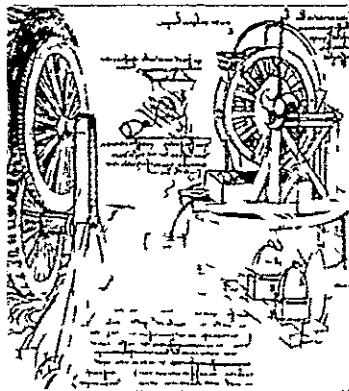


2P

OAKLAND UNIVERSITY SCHOOL OF ENGINEERING



Reproduced by the
CLEARINGHOUSE
for Federal Scientific & Technical
Information Springfield Va 22151

N69-36433	
(ACCESSION NUMBER)	(THRU)
<u>51</u> (PAGES)	<u>1</u> (CODE)
<u>CR105653</u> (NASA CR OR TMX OR AD NUMBER)	<u>04</u> (CATEGORY)

FACILITY FORM 602

FIRST QUARTERLY PROGRESS REPORT

on

ERC/NASA

Contract No. NGR 23-054-003 O.U. Account No. 24771

BIOSYSTEMS ENGINEERING RESEARCH

30 July 1969

School of Engineering
Oakland University
Rochester, Michigan 48063

J. E. Gabson, Principal Investigator
R. H. Edgerton
R. E. Haskell
J. C. Hill

FIRST QUARTERLY PROGRESS REPORT

on

ERC/NASA

Contract No. NGR 23-054-003

BIOSYSTEMS ENGINEERING RESEARCH

J. E. Gibson, Principal Investigator

J. C Hill

R. E. Haskell

R. H Edgerton

School of Engineering

Oakland University

Rochester, Michigan 48063

INTRODUCTION

Considerable progress has been made during the first quarter of this contract.

The work led by J. C Hill on postural control has led to a deviation of the equations of motion for a seven-element stick man. Work has been initiated on an experimental determination of the force-velocity characteristics of human muscles.

Some concern has been expressed about the relationship to the mission of NASA of our proposed work on Bio-optics. For this reason support for this activity was limited to one man month and the object set of defining the proposed area for research. The section of this proposal entitled Bio-optics will satisfy this need, we feel.

One of the major areas of work in this effort is to be Biological Pattern Recognition. An interesting start has been made using the techniques of coherent optics and optical data processing. We wish especially to call the attention of ERC to the increase in speed of pattern recognition which is theoretically possible in this approach.

The work on describing function analysis of man/machine systems is continuing in the final phase of an NSF research initiation grant. This grant will be completed in August of 1969 and no charges have been made for this work as yet on the present grant. The final report to NSF will be forwarded to ERC in September, 1969.

Chapter I.

POSTURAL CONTROL SYSTEM

I. Progress to Date

- a. The equations of motion of the seven-element stick man depicted in Figure 1 are being derived by means of Lagrange's equations. In terms of the generalized coordinates indicated in Figure 1, the total system kinetic energy may be expressed as the sum of the point mass kinetic energy and the kinetic energy due to the distributed nature of the arms, legs, etc.,

$$T = T_{\text{DIST}} + T_{\text{POINT}} \quad (1)$$

The distributed kinetic energy is due only to rotation of the various elements, and is easily obtained as

$$\begin{aligned} T_{\text{DIST}} = & 1/2 J_{\text{TR}} \dot{\theta}^2 + 1/2 J_{\text{HD}} (\dot{\theta} + \dot{\zeta})^2 + 1/2 J_{\text{UA}} (\dot{\theta} - \dot{\delta})^2 \\ & + 1/2 J_{\text{FA}} (\dot{\theta} - \dot{\delta} - \dot{\epsilon})^2 + 1/2 J_{\text{TH}} (\dot{\theta} - \dot{\gamma})^2 \\ & + 1/2 J_{\text{SH}} (\dot{\theta} - \dot{\delta} + \dot{\beta})^2 + 1/2 J_{\text{FT}} (\dot{\theta} - \dot{\gamma} + \dot{\beta} + \dot{\alpha})^2 \end{aligned} \quad (2)$$

The kinetic energy due to the point masses is more difficult to obtain, as it involves repetitive application of the relative velocity theorem together with a long chain of coordinate resolutions to enable expression of the kinetic energy of each point mass in the form

$$T = 1/2M(V_a^2 + V_b^2)$$

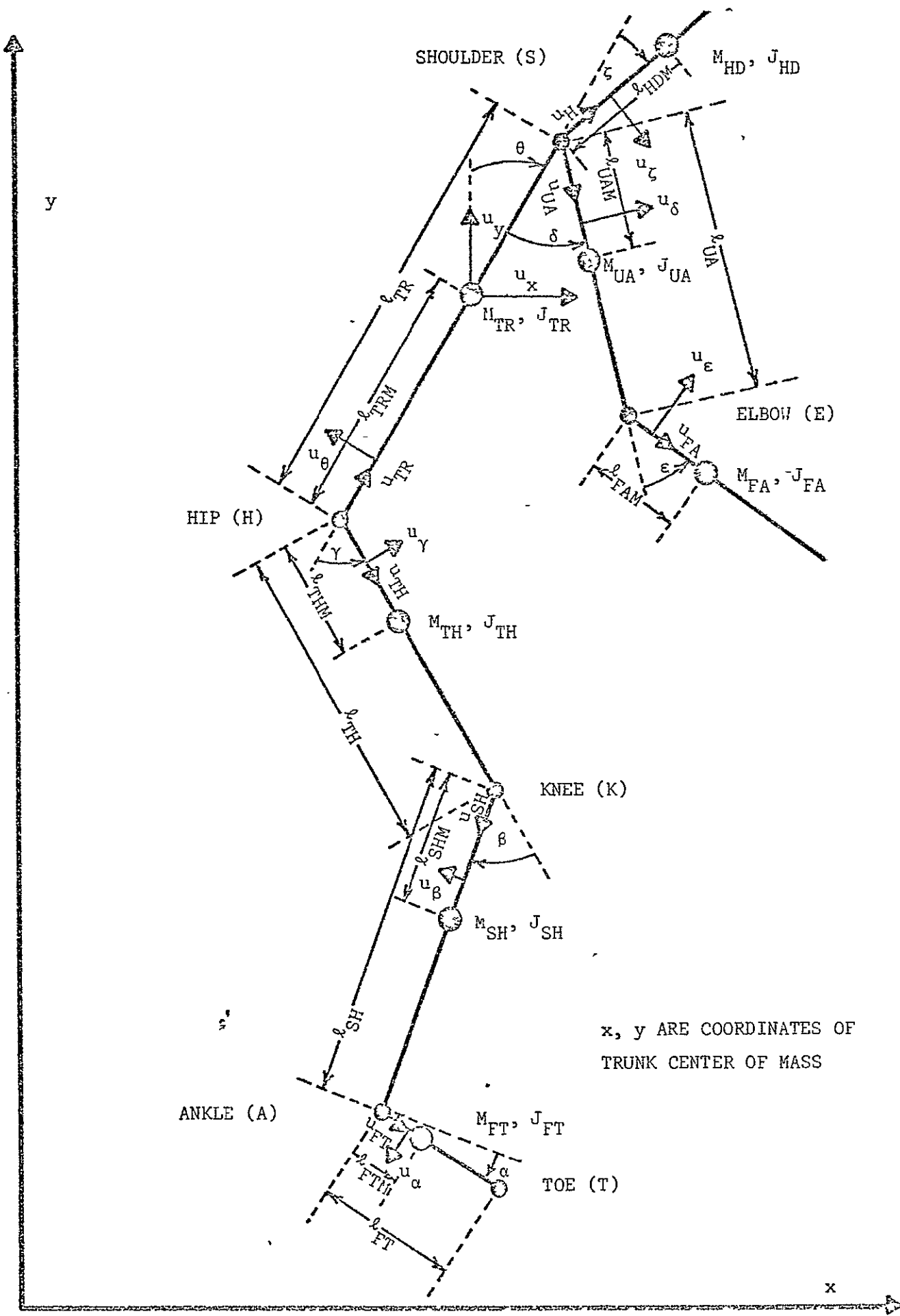


Figure 1. Stickman

where V_a and V_b are velocity components along any set of perpendicular axes. A tentative derivation of the V_a, V_b components for each of the masses follows. The absolute velocity of, say, the c.g. of the trunk is denoted by $\dot{V}_{TR/O}$, while the relative velocity of, say, the hip with respect to the c.g. of the trunk is denoted by $\dot{V}_{H/TR}$.

Unit vectors in a variety of directions are indicated on the diagram, and are denoted by, for example, \hat{U}_x and \hat{U}_y .

The velocity components of each mass point must now be obtained along any convenient set of orthogonal axes, the choice of which varies during the analysis. We have

$$\dot{V}_{TR/O} = \dot{x}\hat{U}_x + \dot{y}\hat{U}_y \quad (3)$$

$$\dot{V}_{H/TR} = l_{TRM} \dot{\theta} \hat{U}_{\theta} \quad (4)$$

Using the relative velocity theorem, the absolute velocity of the hip can be expressed as the relative velocity of the hip with respect to the c.g. of the trunk plus the absolute velocity of the trunk:

$$\begin{aligned} \dot{V}_{H/O} &= \dot{V}_{H/TR} + \dot{V}_{TR/O} \\ &= l_{TRM} \dot{\theta} \hat{U}_{\theta} + \dot{x}\hat{U}_x + \dot{y}\hat{U}_y \end{aligned} \quad (5)$$

Resolving into $\hat{U}_{\theta}, \hat{U}_{TR}$ coordinates so that the vector addition can be performed

$$\begin{aligned}
\dot{V}_{H/O} &= l_{TRM} \dot{\theta} U_{\theta} + [-\dot{x} \cos \theta + \dot{y} \sin \theta] U_{\theta} \\
&+ [\dot{x} \sin \theta + \dot{y} \cos \theta] U_{TR} \\
&= [l_{TRM} \dot{\theta} - \dot{x} \cos \theta + \dot{y} \sin \theta] U_{\theta} \\
&+ [\dot{x} \sin \theta + \dot{y} \cos \theta] U_{TR} \\
&= V_{H\theta} U_{\theta} + V_{HTR} U_{TR}
\end{aligned} \tag{6}$$

$$\begin{aligned}
\dot{V}_{TH/O} &= \dot{V}_{TH/H} + \dot{V}_{H/O} \\
&= l_{THM} \dot{\gamma} U_{\gamma} + \dot{V}_{H/O} \\
&= l_{THM} \dot{\gamma} U_{\gamma} + V_{H\theta} U_{\theta} + V_{HTR} U_{TR} \\
&= l_{THM} \dot{\gamma} U_{\gamma} + [l_{TRM} \dot{\theta} - \dot{x} \cos \theta + \dot{y} \sin \theta] U_{\theta} \\
&+ [\dot{x} \sin \theta + \dot{y} \cos \theta] U_{TR}
\end{aligned} \tag{7}$$

Resolving into U_{γ} , U_{TH} coordinates,

$$\begin{aligned}
\dot{V}_{TH/O} &= l_{THM} \dot{\gamma} U_{\gamma} + [-V_{HTR} \cos \gamma - V_{H\theta} \sin \gamma] U_{TH} + [-V_{H\theta} \cos \gamma + V_{HTR} \sin \gamma] U_{\gamma} \\
&= l_{THM} \dot{\gamma} U_{\gamma} + [-(\dot{x} \sin \theta + \dot{y} \cos \theta) \cos \gamma \\
&- (l_{TRM} \dot{\theta} - \dot{x} \cos \theta + \dot{y} \sin \theta) \sin \gamma] U_{TH} \\
&+ [-(l_{TRM} \dot{\theta} - \dot{x} \cos \theta + \dot{y} \sin \theta) \cos \gamma \\
&+ (\dot{x} \sin \theta + \dot{y} \cos \theta) \sin \gamma] U_{\gamma}
\end{aligned}$$

$$\begin{aligned}
&= [l_{THM} \dot{\gamma} - (l_{TRM} \dot{\theta} - \dot{x} \cos \theta + \dot{y} \sin \theta) \cos \gamma \\
&+ (\dot{x} \sin \theta + \dot{y} \cos \theta) \sin \gamma] U_{\gamma} \\
&+ [-(\dot{x} \sin \theta + \dot{y} \cos \theta) \cos \gamma \\
&- (l_{TRM} \dot{\theta} - \dot{x} \cos \theta + \dot{y} \sin \theta) \sin \gamma] U_{TH} \\
&+ V_{TH\gamma} U_{\gamma} + V_{THH\gamma TH} U_{TH}
\end{aligned} \tag{8}$$

The absolute velocity of the knee is given by

$$\begin{aligned}
V_{K/O} &= V_{K/H} + V_{H/O} \\
&= [l_{TH} \dot{\gamma} - (l_{TRM} \dot{\theta} - \dot{x} \cos \theta + \dot{y} \sin \theta) \cos \gamma \\
&+ (\dot{x} \sin \theta + \dot{y} \cos \theta) \sin \gamma] U_{\gamma} \\
&+ [-(\dot{x} \sin \theta + \dot{y} \cos \theta) \cos \gamma - (l_{TRM} \dot{\theta} - \dot{x} \cos \theta + \dot{y} \sin \theta) \sin \gamma] U_{TH}
\end{aligned} \tag{9}$$

The absolute velocity of the center of the mass of the shank is given by

$$\begin{aligned}
V_{SH/O} &= V_{SH/K} + V_{K/O} \\
&= l_{SHM} \dot{\beta} U_{\beta} + V_{K/O}
\end{aligned}$$

$$\begin{aligned}
&= \{ \dot{l}_{SHM}^{\beta} + [\dot{l}_{TH}^{\gamma} - (\dot{l}_{TRM}^{\theta} - \dot{x} \cos \theta + \dot{y} \sin \theta) \cos \gamma] \cos \beta \\
&- [- \dot{x} \sin \theta + \dot{y} \cos \theta] \cos \gamma \\
&- (\dot{l}_{TRM}^{\theta} - \dot{x} \cos \theta + \dot{y} \sin \theta) \sin \beta \} U_{\beta} \\
&+ \{ [- (\dot{x} \sin \theta + \dot{y} \cos \theta) \cos \gamma - (\dot{l}_{TRM}^{\theta} - \dot{x} \cos \theta \\
&+ \dot{y} \sin \theta) \sin \gamma] \cos \beta - [\dot{l}_{TH}^{\gamma} - (\dot{l}_{TRM}^{\theta} - \dot{x} \cos \theta \\
&+ \dot{y} \sin \theta) \cos \gamma + (\dot{x} \sin \theta + \dot{y} \cos \theta) \sin \gamma] \sin \beta \} U_{SH} \quad (10)
\end{aligned}$$

The absolute velocity of the ankle is obtained by substituting \dot{l}_{SH} for \dot{l}_{SHM} in equation (10), giving

$$\begin{aligned}
V_{A/O} &= \{ \dot{l}_{SH}^{\beta} + [\dot{l}_{TH}^{\gamma} - (\dot{l}_{TRM}^{\theta} - \dot{x} \cos \theta + \dot{y} \sin \theta) \cos \gamma] \cos \beta \\
&- [- (\dot{x} \sin \theta + \dot{y} \cos \theta) \cos \gamma - (\dot{l}_{TRM}^{\theta} - \dot{x} \cos \theta + \dot{y} \sin \theta) \\
&\sin \beta] U_{\beta} + \{ [- (\dot{x} \sin \theta + \dot{y} \cos \theta) \cos \gamma \\
&- (\dot{l}_{TRM}^{\theta} - \dot{x} \cos \theta + \dot{y} \sin \theta) \sin \gamma] \cos \beta - [\dot{l}_{TH}^{\gamma} \\
&- (\dot{l}_{TRM}^{\theta} - \dot{x} \cos \theta + \dot{y} \sin \theta) \cos \gamma + (\dot{x} \sin \theta + \dot{y} \cos \theta) \sin \gamma] \sin \beta \} U_{SH} \\
&= V_{aO\beta} U_{\beta} + V_{aOSH} U_{SH} \quad (11)
\end{aligned}$$

$$\begin{aligned}
V_{FT/O} &= V_{FT/A} + V_{A/O} \\
&= \dot{l}_{FTM}^{\alpha} U_{\alpha} + V_{A/O}
\end{aligned}$$

Resolving equation (11) into U_{α} , U_{SH} coordinates, the absolute velocity of the c.g. of the foot is

$$\begin{aligned}
\dot{V}_{FT/O} &= l_{FTM} \dot{\alpha} U_{\alpha} + [V_{aOSH} \cos \alpha + V_{aO\beta} \sin \alpha] U_{\alpha} \\
&+ [-V_{aO\beta} \cos \alpha + V_{aOSH} \sin \alpha] U_{SH} \\
&= l_{FTM} \dot{\alpha} U_{\alpha} + \{ [(-\dot{x} \sin \theta + \dot{y} \cos \theta) \cos \gamma - (l_{TRM} \dot{\theta} \\
&- \dot{x} \cos \theta + \dot{y} \sin \theta) \sin \gamma] \cos \beta - [l_{TH} \dot{\gamma} - (l_{TRM} \dot{\theta} \\
&- \dot{x} \cos \theta + \dot{y} \sin \theta) \cos \gamma + (x \sin \theta + \dot{y} \cos \theta) \sin \gamma] \sin \beta \} \cos \alpha \\
&+ \{ l_{SH} \dot{\beta} + [l_{TH} \dot{\gamma} - (l_{TRM} \dot{\theta} - \dot{x} \cos \theta + \dot{y} \sin \theta) \cos \gamma] \cos \beta \\
&- [(-\dot{x} \sin \theta + \dot{y} \cos \theta) \cos \gamma - (l_{TRM} \dot{\theta} - \dot{x} \cos \theta + \dot{y} \sin \theta) \sin \beta] \sin \alpha \} U_{\alpha} \\
&+ \{ -[l_{SH} \dot{\beta} + [l_{TH} \dot{\gamma} - (l_{TRM} \dot{\theta} - \dot{x} \cos \theta + \dot{y} \sin \theta) \cos \gamma] \cos \beta \\
&- [(-\dot{x} \sin \theta + \dot{y} \cos \theta) \cos \gamma - (l_{TRM} \dot{\theta} - \dot{x} \cos \theta + \dot{y} \sin \theta) \sin \beta] \} \cos \alpha \\
&+ \{ -(-\dot{x} \sin \theta + \dot{y} \cos \theta) \cos \gamma - (l_{TRM} \dot{\theta} - \dot{x} \cos \theta + \dot{y} \sin \theta) \sin \gamma \} \cos \beta \\
&- [l_{TH} \dot{\gamma} - (l_{TRM} \dot{\theta} - \dot{x} \cos \theta + \dot{y} \sin \theta) \cos \gamma + (\dot{x} \sin \theta + \dot{y} \cos \theta) \sin \gamma] \\
&\sin \beta \} \sin \alpha \} U_{SH} \tag{12}
\end{aligned}$$

Expressions for the absolute velocities of the shoulder, upperarm, and forearm are obtained in similar fashion

$$\begin{aligned}
\dot{V}_{S/O} &= \dot{V}_{S/TR} + \dot{V}_{TR/O} \\
&= -(l_{TR} - l_{TRM}) \dot{\theta} U_{\theta} + \dot{x} U_{\alpha} + \dot{y} U_{\gamma} \tag{13}
\end{aligned}$$

Resolving into U_{θ} , U_{TR} coordinates, the absolute velocity of the shoulder is obtained as

$$\begin{aligned}
\dot{V}_{S/O} &= -(\dot{l}_{TR} - \dot{l}_{TRM})\dot{\theta} U_{\theta} + [-\dot{x} \cos\theta + \dot{y} \sin\theta] U_{\theta} \\
&+ [\dot{x} \sin\theta + \dot{y} \cos\theta] U_{TR} \\
&= [-(\dot{l}_{TR} - \dot{l}_{TRM})\dot{\theta} - \dot{x} \cos\theta + \dot{y} \sin\theta] U_{\theta} \\
&+ [\dot{x} \sin\theta + \dot{y} \cos\theta] U_{TR}
\end{aligned} \tag{14}$$

The velocity of the c g of the upper arm is then given by equation (15).

$$\begin{aligned}
\dot{V}_{UA/O} &= \dot{V}_{UA/S} + \dot{V}_{S/O} \\
&= \dot{l}_{UAM}\dot{\delta} U_{\delta} + \dot{V}_{S/O} \\
&= \dot{l}_{UAM}\dot{\delta} U_{\delta} + [-(\dot{l}_{TR} - \dot{l}_{TRM})\dot{\theta} - \dot{x} \cos\theta + \dot{y} \sin\theta] U_{\theta} \\
&+ [\dot{x} \sin\theta + \dot{y} \cos\theta] U_{TR}
\end{aligned} \tag{15}$$

Resolving into U_{δ} , U_{UA} coordinates gives

$$\begin{aligned}
\dot{V}_{UA/O} &= \dot{l}_{UAM}\dot{\delta} U_{\delta} + \{[-(\dot{l}_{TR} - \dot{l}_{TRM})\dot{\theta} - \dot{x} \cos\theta + \dot{y} \sin\theta] \sin\delta \\
&- [\dot{x} \sin\theta + \dot{y} \cos\theta] \cos\delta\} U_{\delta} \\
&+ \{[(\dot{l}_{TR} - \dot{l}_{TRM})\dot{\theta} - \dot{x} \cos\theta + \dot{y} \sin\theta] \cos\delta + [\dot{x} \sin\theta + \dot{y} \cos\theta] \sin\delta\} U_{UA} \\
&= \dot{l}_{UAM}\dot{\delta} + [-(\dot{l}_{TR} - \dot{l}_{TRM})\dot{\theta} - \dot{x} \cos\theta + \dot{y} \sin\theta] \sin\delta \\
&- [\dot{x} \sin\theta + \dot{y} \cos\theta] \cos\delta\} U_{\delta} \\
&+ \{[(\dot{l}_{TR} - \dot{l}_{TRM})\dot{\theta} - \dot{x} \cos\theta + \dot{y} \sin\theta] \cos\delta + [\dot{x} \sin\theta + \dot{y} \cos\theta] \sin\delta\} U_{UA}
\end{aligned} \tag{16}$$

The elbow velocity is obtained by replacing l_{UAM} in equation (16) by l_{UA}

$$\begin{aligned}
 \dot{V}_{E/O} = & l_{UA} \dot{\delta} + [-(l_{TR} - l_{TRM}) \dot{\theta} - \dot{x} \cos \theta + \dot{y} \sin \theta] \sin \delta \\
 & - [x \sin \theta + y \cos \theta] \cos \delta \dot{U}_{\delta} + [(l_{TR} - l_{TRM}) \dot{\theta} \\
 & - \dot{x} \cos \theta + \dot{y} \sin \theta] \cos \delta + [\dot{x} \sin \theta + y \cos \theta] \sin \delta \dot{U}_{UA} \quad (17)
 \end{aligned}$$

The velocity of the forearm c.g. is obtained by the relative velocity theorem as

$$\begin{aligned}
 \dot{V}_{FA/O} = & \dot{V}_{FA/E} + \dot{V}_{E/O} \\
 = & l_{FAM} \dot{\epsilon} U_{\epsilon} + \dot{V}_{E/O} \quad (18)
 \end{aligned}$$

Resolving into U_{ϵ} , U_{FA} coordinates yields

$$\begin{aligned}
 \dot{V}_{FA/O} = & l_{FAM} \dot{\epsilon} U_{\epsilon} + \{ [l_{UA} \dot{\delta} + [-(l_{TR} - l_{TRM}) \dot{\theta} - x \cos \theta \\
 & + y \sin \theta] \sin \delta - [\dot{x} \sin \theta + \dot{y} \cos \theta] \cos \delta \} \cos \epsilon - [(l_{TR} - l_{TRM}) \dot{\theta} \\
 & - \dot{x} \cos \theta + \dot{y} \sin \theta] \cos \delta + [x \sin \theta + y \cos \theta] \sin \delta \dot{U}_{\epsilon} \\
 & + \{ [l_{UA} \dot{\delta} + [-(l_{TR} - l_{TRM}) \dot{\theta} - \dot{x} \cos \theta + \dot{y} \sin \theta] \sin \delta \\
 & - [x \sin \theta + \dot{y} \cos \theta] \cos \delta \} \sin \epsilon + [(l_{TR} - l_{TRM}) \dot{\theta} \\
 & - \dot{x} \cos \theta + \dot{y} \sin \theta] \cos \delta + [x \sin \theta + \dot{y} \cos \theta] \sin \delta \dot{U}_{FA}
 \end{aligned}$$

$$\begin{aligned}
&= \{l_{FAM} \dot{\epsilon} + [l_{UA} \dot{\delta} + [-(l_{TR} - l_{TRM}) \dot{\theta} - \dot{x} \cos\theta \\
&+ \dot{y} \sin\theta] \sin\delta - [x \sin\theta + y \cos\theta] \cos\delta] \cos\epsilon \\
&- [(l_{TR} - l_{TRM}) \dot{\theta} - \dot{x} \cos\theta + y \sin\theta] \cos\delta + [\dot{x} \sin\theta + \dot{y} \cos\theta] \\
&\sin\delta] \sin\epsilon \}_{U_{\epsilon}} + [l_{UA} \dot{\delta} + [-(l_{TR} - l_{TRM}) \dot{\theta} \\
&- \dot{x} \cos\theta + y \sin\theta] \sin\delta - [x \sin\theta + y \cos\theta] \cos\delta] \sin\epsilon \\
&+ \{[(l_{TR} - l_{TRM}) \dot{\theta} - \dot{x} \cos\theta + \dot{y} \sin\theta] \cos\delta + [\dot{x} \sin\theta + \dot{y} \cos\theta] \\
&\sin\delta] \cos\epsilon \}_{U_{\delta}}
\end{aligned} \tag{19}$$

Finally, the absolute velocity of the head c.g. is given by

$$\begin{aligned}
V_{HD/O} &= V_{HD/S} + V_{S/O} \\
&= l_{HDM} \dot{\zeta} U_{\delta} + V_{S/O}
\end{aligned} \tag{20}$$

Resolving into U_{δ} , U_{HD} coordinates,

$$\begin{aligned}
V_{HD/O} &= l_{HDM} \dot{\zeta} U_{\delta} + \{[-(l_{TR} - l_{TRM}) \dot{\theta} - x \cos\theta + \dot{y} \sin\theta] \cos\zeta \\
&- [\dot{x} \sin\theta + \dot{y} \cos\theta] \sin\zeta\} U_{\zeta} + \{[-(l_{TR} - l_{TRM}) \dot{\theta} \\
&- \dot{x} \cos\theta + \dot{y} \sin\theta] \sin\zeta + [x \sin\theta + y \cos\theta] \cos\zeta\} U_{HD} \\
&= \{l_{HDM} \dot{\delta} - [-(l_{TR} - l_{TRM}) \dot{\theta} - \dot{x} \cos\theta + \dot{y} \sin\theta] \cos\zeta \\
&- [x \sin\theta + \dot{y} \cos\theta] \sin\zeta\} U_{\zeta} + \{[-(l_{TR} - l_{TRM}) \dot{\theta} \\
&- x \cos\theta + \dot{y} \sin\theta] \sin\zeta + [x \sin\theta + \dot{y} \cos\theta] \cos\zeta\} U_{HD}
\end{aligned} \tag{21}$$

Equations (3), (8), (10), (12), (16), (19), and (21) give the velocity components of the trunk, thigh, shank, foot, upper arm, forearm, and head respectively, these components are obtained in several different coordinate systems

The velocity components must now be squared, added, and eventually partially differentiated. The expressions are uncomfortably lengthy for manipulation by hand, although not yet impossibly so.

b. The force-velocity characteristics of human muscles will appear in the generalized forces when these are derived for the equations of motion. A fixture to allow gathering of experimental data on these characteristics for the shoulder extensor and the biceps has been constructed, and is being used to provide verification of the dominant properties of these muscles as previously reported in the literature. A relatively small part of the research effort has been devoted to this area up to the present time.

II. Future Work on Postural Control System

a. A way of deriving the equations of motion more effective and reliable than hand manipulation is being sought. The symbolic manipulation capabilities of the FORMAC digital computer program will be evaluated for possible use in the problem of obtaining expressions for the system kinetic energies. A program called COSMIC 160, which performs analytic differentiation, is being evaluated for possible application to the partial differentiation phase of the Lagrangian formulation.

b Work on the measurement of the force-velocity characteristics of human muscle will continue.

Chapter II.

BIO-OPTICS

This report represents progress to date of work on two aspects related to bio-optics the first is to provide a design of a continuously variable focusing system which could be used either

- a) to replace bifocal lenses
- b) allow bifocal contact lenses, or
- c) provide an artificial cornea.

the second is an attempt to describe and model the cornea

The application of liquid crystals for these purposes was tentatively chosen as a media because of their sensitive optical properties which can be readily altered by magnetic, electrical or mechanical means (1,2,3)

Introduction to Spectacle Requirements

To discuss the requirements of a controlled focus system for spectacle wearers, some rough calculations will be presented in this section

The relation of the index refraction to the dielectric constant and the permeability in the media is known to be related through Maxwell's equations

$$n = \left(\frac{\epsilon}{\epsilon_0} \frac{\mu}{\mu_0} \right)^{1/2}$$

If the media is nonmagnetic the permeability $\mu = \mu_0$, (ϵ_0 = the permittivity of vacuum) then $n = \left(\frac{\epsilon}{\epsilon_0}\right)^{1/2} = (k)^{1/2}$ where k is the dielectric constant. Thus, if as observed by Carr⁽¹⁾, $\frac{K_E}{K_0}$ of 1.12 are observable in thin films then

$$\frac{n_E}{n_0} = \left(\frac{K_E}{K_0}\right)^{1/2} = \left(\frac{3.7}{3.3}\right)^{1/2} = 1.07$$

is readily obtained with nematic (liquid crystal) substances. Since optical focal length of a lense is expressed as

$$f = \frac{\text{radius of curvature}}{(n-n_0)}$$

if $n_E = 1.07$ and $n_0 = 1$ is taken as the index of refraction for air then

$$\frac{f_E}{f_0} = \frac{n_0 - 1}{n_E - 1} = \frac{n_0 - 1}{1.07 n_0 - 1}$$

if $n_0 = \sqrt{3.3}$ then

$$\frac{f_E}{f_0} = \frac{1.82 - 1}{(1.07)(1.82) - 1} = \frac{82}{95} = 0.86$$

The focal length can thus be changed by 14%. This must be compared with the accommodation of the lense. If $\frac{f_E}{f_0} = 0.86$ then the focal power

$$D \equiv \frac{1}{f}$$

$$\frac{D_0}{D_E} = 0.86$$

D_o , the focal power of the cornea is roughly 50 diopters or

$$D_E = \frac{D_o}{.86} = \frac{50}{.86} = 59$$

Then $D_E - D_o = 59 - 50 = 9$ diopters of change is possible. From Fig. (1) the physiological accommodation as a function of age for people goes from 16 to 1 diopters. If a change of 9 is possible this would extend the accommodation of a 68 year old to the equivalent of say an average 30 year old

- In practice, spectacles for continuous use are prescribed as 2/3 the power needed for reading at 40 cm. Thus a reading lense of bifocal of 1/3 the total power is often prescribed. If a conventional lense were to take the $(\frac{2}{3}) 15 = 10$ diopters, then a controlled variation of 5 diopters could easily be supplied with a liquid crystal effect.

The problem then is to change the index of refraction by a simple means. The orientation of long molecules by electrical, magnetic and active surfaces as well as shear are possible with nematic (thread like) liquid crystals which in turn changes the index of refraction. Surface orientation can be achieved with p-azoxyanisole by rubbing the surface of a glass sandwich with a cloth in one direction (the direction of orientation desired). Then by one of the field effects described this can then be altered or alternatively starting from a random dispersion the fields can be used for alignment. The concern in the present research for using shear induced index of refraction changes rather than electrical or magnetic is that the possibility exists for control of the index at positions remote from the driving mechanism. For example,

vibration of one surface while the other is fixed is simpler than applying a magnetic field perpendicular to the surfaces

Electrically conducting transparent materials for a sandwich material are also being sought but so far the only materials which have been obtained are tin oxide coated glass. It is felt that electrically conductive plastics are a possible material for use in this application if satisfactory materials can be obtained

The other reason for examining the flow or shear effects is the possibility of utilizing the dynamic scattering mode⁽³⁾ for refraction change. In this case the hydrodynamic effects must be understood to develop a design

The analysis of the index of refraction change in the static field situation has been made, by Fricke⁽⁵⁾. This analysis has been extended to the shear situation shown in Figure (2) this summer starting from the analysis of the conductivity of a suspension of ellipsoids representing molecules

Theoretical calculations on the change in dielectric constant for a sheared suspension of particles of symmetrical ellipsoidal shape have been completed. The axis ratio for oblate and prolate ellipsoids was varied and computation of the form factor F_1 relating the dielectric constant for a sheared suspension to the principle dielectric constants for a completely aligned suspension defined by

$$\bar{K}_{11} = K_b + (K_a - K_b)F_1$$

$$\bar{K}_{22} = K_b + (K_a - K_b)F_2$$

$$\bar{K}_{33} = K_b + (K_a - K_b)F_3$$

have been theoretically computed. The computer calculations for the factor F_3 have been completed and are shown plotted in Figure (3)

Similar calculations are in progress for F_2 and F_1

In the limit of large axis ratio $r = \frac{a}{b}$ or very long rods ($r \rightarrow \infty$) these are analytically evaluated as

$$F_1 = \frac{\ln 2}{\pi}, \quad F_2 = 0, \quad F_3 = \frac{1}{2}$$

Since the factor F_1 is $\frac{1}{2}$ for a random angular distribution of particles, it is easily seen that for long molecules the effect of shear produced by motion parallel to the X_1' axis produces theoretically no change in the dielectric constant in the X_3' direction. Vibration of two plates parallel to each other is not therefore an effective way of producing index of refraction changes perpendicular to the plates. An effective way to produce a change is to shear the material in the plane and observe the change parallel to the shear planes. Thus variation will be observed in K_{22} as a result of shear parallel to the X_1' axis. In this case for long rods $F_2 = 0$ and the effect is equivalent to complete alignment with rods rotating in the plane.

* K_a and K_b are the dielectric constants for fields parallel to the ellipsoidal axes and a and b respectively where a is the symmetric axis

A sandwich cell has been constructed to test the electrical field and shear field effects on p-azoxyanisole nematic crystals. The recent availability of room temperature materials will assist considerably in these experiments. Experiments with a membrane of liquid crystal supported by surface tension and attached to a piezoelectric crystal proved unsuccessful because of the inability to control the liquid crystal consistency and obtain well defined shear waves.

A fused quartz shear plate is presently under construction to provide better defined shear waves in a sandwich construction setup. A sandwich construction was selected since it appears that for production of a variable index of refraction optical system this type will be required. The later introduction of a curved sandwich is expected if the results of the flat sandwich are promising.

The following three lines of research on this application are expected to be pursued to continue this investigation.

1. To examine the shear effects experimentally it is planned to complete construction of the fused quartz shear generator. This will allow the study of the shear index control possible.

2. The theoretical analysis of dielectric constant variation at optical frequency is expected to be completed including calculation of the dielectric factors F_1 and F_2 for a range of axis ratios.

3. Construction of a controlled index lense will then be attempted if several difficulties involving spherical rather than flat or cylindrical geometry can be circumvented.

Corneal model and analysis

This section of research principally revolves around an explanation for the transparency of the cornea. The present explanations of cornea transparency are based on a "theory" evolved from the calculations based on scattering from small cylindrical fibers shown in Fig. (4) which predict that the cornea should scatter roughly 90% of the light and hence be opaque⁽⁶⁾. The "theory" hypothesizes a lattice which in effect increases the size of the scattering units. It is well known that scattering in the cornea can be increased by mechanical shear or pressure effects⁽⁶⁾. To start with therefore, several pig's eyes were examined, and pressurized by inserting a hypodermic needle through the optic nerve and increasing the pressure in the intact eye. A general conclusion was that pressure was more effective in producing "cloudiness" than mechanical distortion.

The analogy between liquid crystal behavior and corneal stroma was pursued further to reveal the following possibilities for modeling the cornea or replacing it with liquid crystals.

The mechanical shear properties of the stroma are known⁽⁶⁾ to be non-elastic in the sense that shearing of outer to inner layers is not resisted, demonstrating the liquid behavior of this material.

An optical analogy is also possible from analysis of the scattering of light from the cornea and from liquid crystals in the "Dynamic Scattering Mode". Scattering experiments⁽³⁾ on (nematic) liquid crystals in this mode demonstrate that the crystals behave not as single molecule scattering centers but as bundles so that scattering theory for cylinders

large in diameter compared to the wavelength of light are applicable rather than small. The same may be true for the cornea if as has been postulated from analysis for small cylinders that the cornea should be opaque.

A physical analog of the corneal structure is contemplated utilizing fiber optic sections to simulate the scattering from the corneal fibrils and bundles.

A satisfactory explanation of the corneal transparency would help to assist in the problems of opacity in fibrous structures and the mechanisms by which their transparency can be altered.

It is planned therefore to attempt to model the cornea with a fiber optic system and also to examine further the "dynamic scattering theory" using liquid crystals as a possible explanation for the observed transparency.

References

1. Carr, E. F., "Ordering in Liquid Crystals Owing To Electric and Magnetic Fields" Advances in Chemistry, Series 63, p. 76, American Chemical Society, Washington, D C (1967).
2. Deutch, CH and Keating, P. M , "The Scattering of Coherent Light from Nematic Liquid Crystals in the Dynamic Scattering Mode". Bendix Research Laboratories, preliminary report 1969
3. Hellmeier, G H , Zaroni, L A , and Barton, L. A , Dynamic Scattering A New Electro-optic Effect in Certain Classes of Nematic Liquid Crystals Proc IEEE, vol 56, No 7, p 1162 (1968).
4. Bennett, A. G. and Francis, J. L., " Ametropia and Its Correction In The Eye" (H Davson edition), Academic Press, New York and London, vol 14, p 154
5. Fricke, H , The Electric Conductivity and Capacity of Disperse Systems, Physics, vol. 1, p. 106, (1931)
6. Maurice, D M , The Structure and Transparency of the Cornea, Journal of Physiology, vol 136, No. 2, p. 263, (1957)
7. Jakus, M A , The Fine Structure of The Human Cornea In, "The Structure Of The Eye", (G K Smelser, edition), Academic Press, New York and London

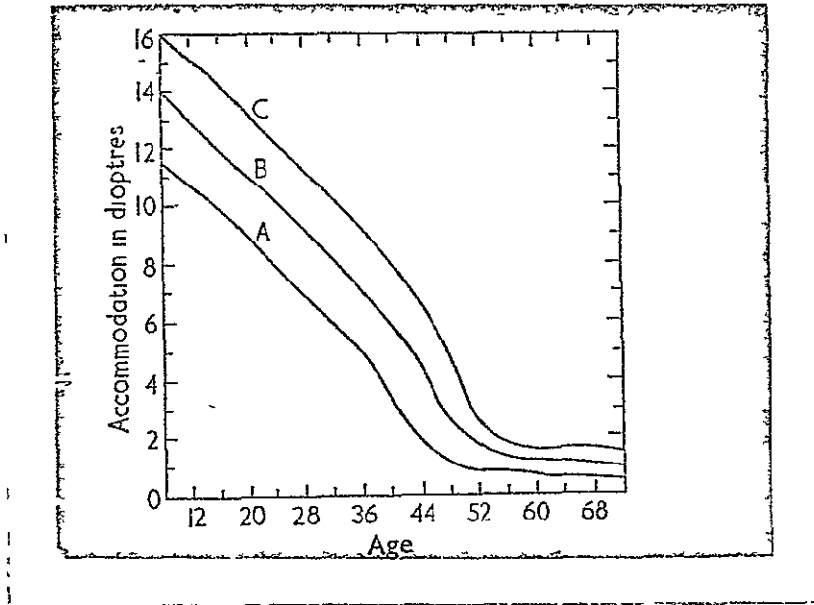
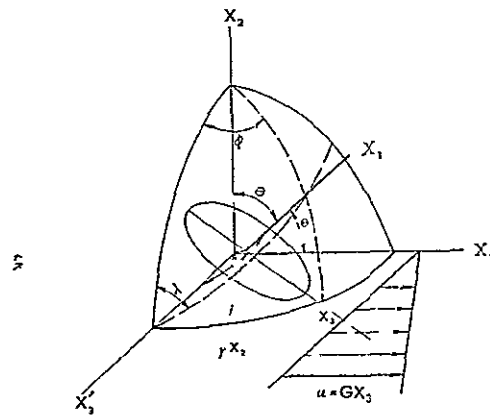


Figure 1 Accomodation of the human eye as a function of age⁽⁴⁾ Curves A and C are physiological limits and B is the normal



COORDINATE GEOMETRY FOR AN ELLIPSOID OF REVOLUTION IN A SHEAR FLOW

Figure 2 Ellipsoid coordinates for a description of particle in a uniform shear field

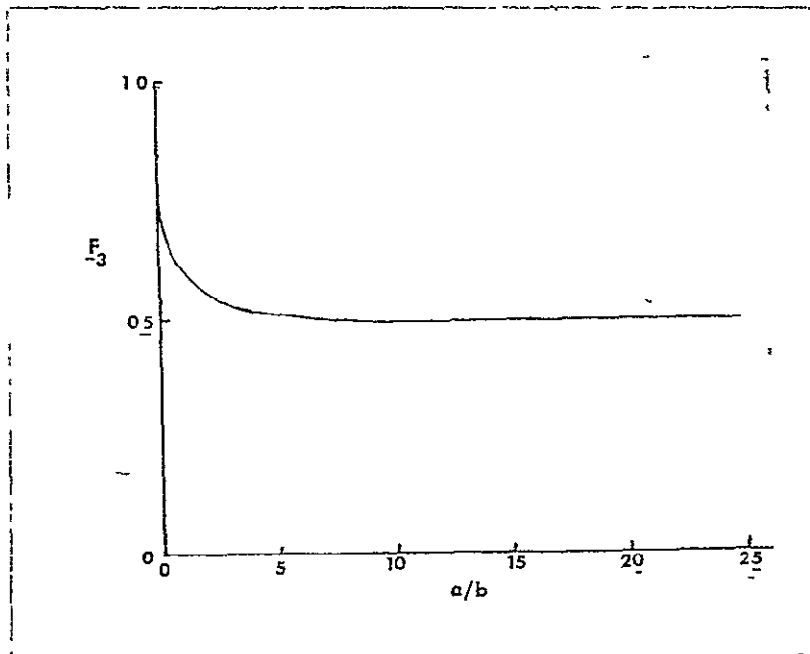


Figure 3 Variation of the form factor for dielectric the constant of a disperse media in a uniform shear field as a function of one axis ratio a/b of symmetrical ellipsoids (a is the axis of symmetry)

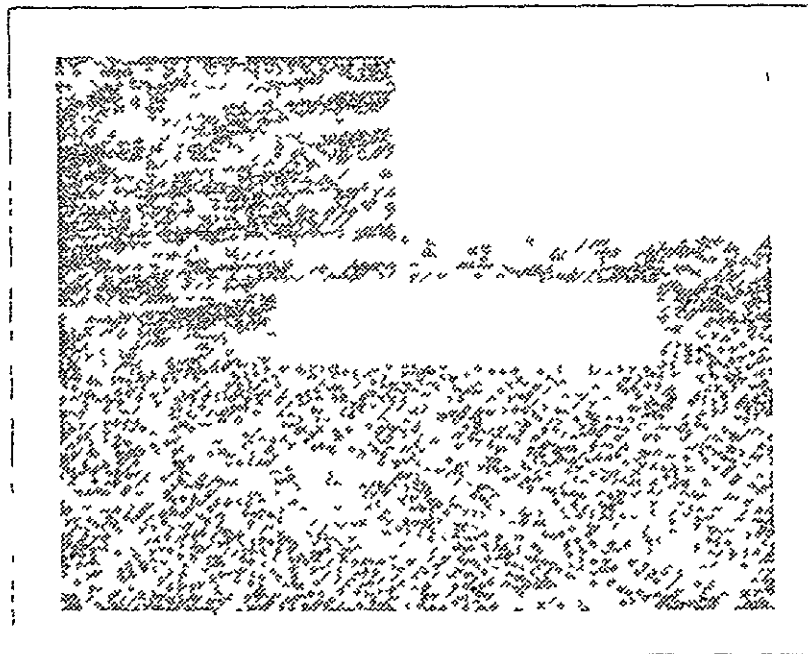


Figure 4 Photo of an X ray micrograph of a section of a cornea sectioned perpendicularly to the surface This photo shows the fibrils located in lamella at different angles in different lamella but very uniform within a lamella Modification of a photo by Jakus⁽⁷⁾

Chapter III.

COHERENT OPTICAL ANALYSIS OF BIOLOGICAL PHOTOMICROGRAPHS

Biological studies remain largely experimental and theories are developed only after a large quantity of experimental data has been collected and analyzed. Major breakthroughs in biology and bio-medicine can be expected only when methods are available which can rapidly analyze this large amount of experimental data in such a way as to suggest mathematical models and physical mechanisms for the particular biological phenomena being studied.

Since the raw data is in the form of biological slides or photomicrographs it is in a form that can be used directly in an optical processing system. This is in sharp contrast to the case of digital computer processing where one would have to convert all of the information in the photomicrograph to digital form before one could begin to process the data. Even if one could put all the information in digital form the time required to carry out the processing even on a fast computer would probably be excessive considering the very large amount of data to be processed. On the contrary the optical processor would carry out the calculations for a single photomicrograph essentially instantaneously (at the speed of light)

Research is being conducted to explore the possibilities of using coherent optical processing techniques for rapidly analyzing large quantities of experimental biological data. The approach is unique in its attempt to characterize biological photomicrographs as random signals from

which quantitative statistical information can be obtained. The information is designed to be in such a form as to suggest mathematical models and physical mechanisms for particular biological phenomena. For example, if a certain cell structure has a particular autocorrelation function it is conceivable that knowing that would suggest some underlying physical theory or mechanism which caused the cell to grow in the manner in which it did. Thus, it might be that such quantitative coherent optical measurement techniques could open up new possibilities in developing mathematical and predictive theories of biological processes. Such techniques could be applied in all areas of biology and medicine and could have far-reaching implications in the understanding of cell growth and disease.

I. Optical Analysis of Biological Photomicrographs

The purpose of this study is to determine what type of quantitative information about a biological photomicrograph can be obtained by considering the amount of light transmitted by the photomicrograph at a given location to be a random variable. The photomicrograph represents a two dimensional random process which acts as a random diffracting screen when illuminated with coherent light. The resulting diffracted light can provide statistical information about the spatial distribution of the photomicrograph image. The progress to date has included an analysis of photomicrographs as random diffracting screens, power spectrum and autocorrelation measurements of some specific photomicrographs and some random test screens, and the design of a new lensless optical processor.

II. Photomicrographs as Random Diffracting Screens

Figure 1 shows coherent light incident from the left on a photomicrograph which is located in the x-y plane and acts as a diffracting screen. If $U(x,y)$ is the complex amplitude of light just to the left of the screen then the light amplitude just to the right of the screen is given by

$$U'(x,y) = g(x,y) U(x,y) \quad (1)$$

where

$$g(x,y) = A(x,y)e^{j\phi(x,y)} \quad (2)$$

is the complex transmittance of the photomicrograph. The amplitude and phase of this transmittance, $A(x,y)$ and $\phi(x,y)$, are considered to be two-dimensional random functions of the coordinates x and y . For convenience

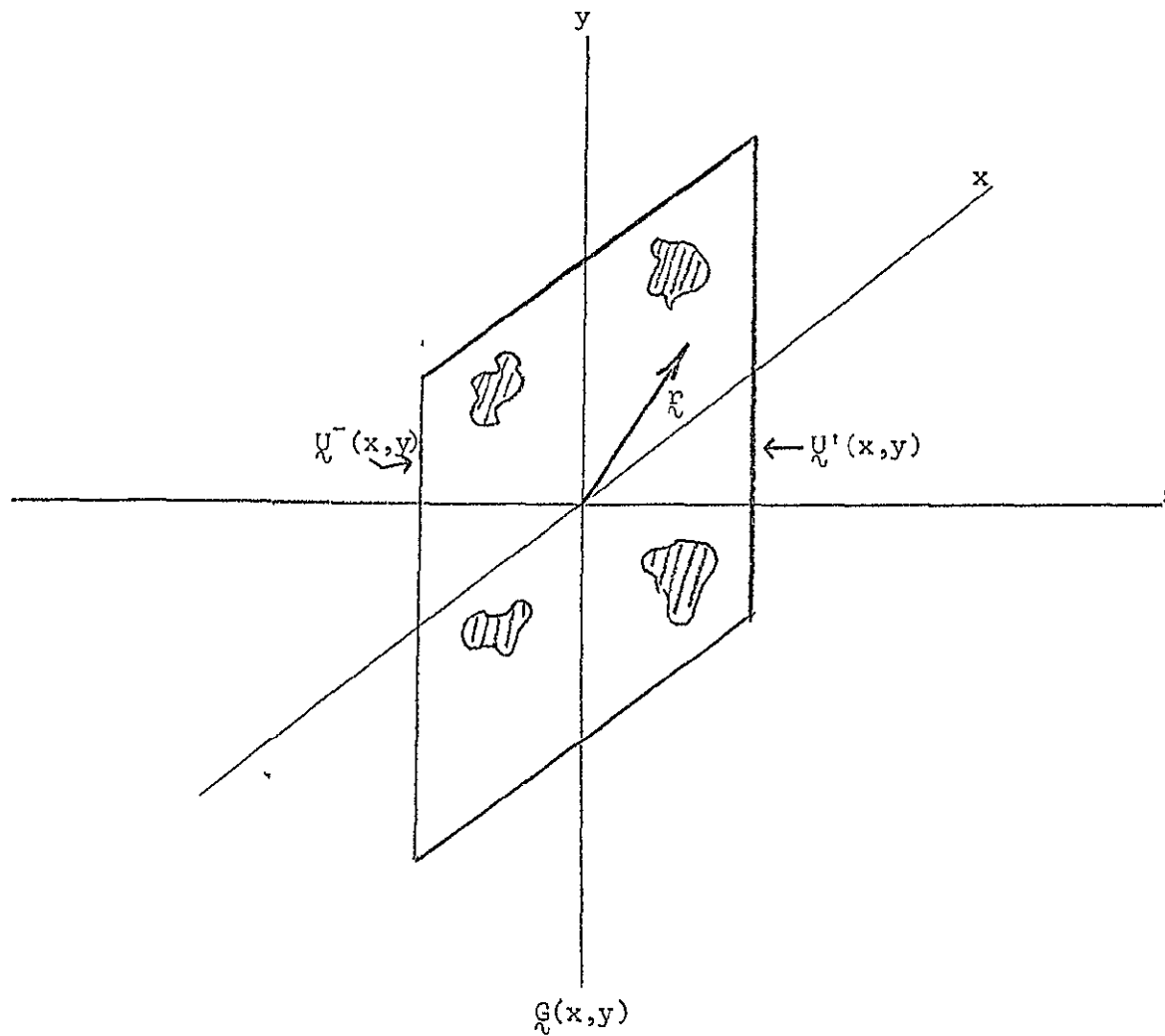


Fig 1
Photomicrograph as a
Random Diffracting Screen

the position vector $r = xu_x + yu_y$ can be introduced so the (2) can be written as

$$g(r) = A(r)e^{j\phi(r)} \quad (3)$$

The random functions $A(r)$ and $\phi(r)$ are characterized by the one-dimensional probability densities $p(a, r)$ and $p(\phi, r)$. Thus, for example, $p(a, r)da$ is the probability that at the position r , the amplitude $A(r)$ has a value between a and $a + da$. These one-dimensional probability densities can be used to find the mean values, variances and higher moments of the random functions $A(r)$ and $\phi(r)$. However, they by no means give a complete description of these random functions. The most important information in the photomicrograph concerns the spatial distribution of the particular objects photographed (cells, nuclei, etc.) The statistical properties of these spatial distributions are characterized by higher order probability density functions. The most important of these are the two-dimensional probability density $p(a_1, a_2, r_1, r_2)$ and $p(\phi_1, \phi_2, r_1, r_2)$. Thus, for example, $p(\phi_1, \phi_2, r_1, r_2)d\phi_1d\phi_2$ is the probability that at the position r_1 the phase $\phi(r_1)$ has a value between ϕ_1 and $\phi_1 + d\phi_1$ and at the position r_2 the phase $\phi(r_2)$ has a value between ϕ_2 and $\phi_2 + d\phi_2$.

These two-dimensional probability densities can be used to calculate the correlation functions $B_A(r_1, r_2)$ and $B_\phi(r_1, r_2)$. Thus, for example

$$\begin{aligned} B_A(r_1, r_2) &= \langle A(r_1)A(r_2) \rangle \\ &= \iint a_1 a_2 p(a_1, a_2, r_1, r_2) da_1 da_2 \end{aligned} \quad (4)$$

A particular photomicrograph will represent a certain realization of the random processes $A(\underline{r})$ and $\Phi(\underline{r})$. The ensemble associated with these random processes might consist of a collection of similar photomicrographs from different specimens or photomicrographs of different regions of the same specimen. The random processes $A(\underline{r})$ and $\Phi(\underline{r})$ are said to be stationary in the wider sense if the expected values $\langle A \rangle$ and $\langle \Phi \rangle$ are independent of \underline{r} and the correlation functions $B_A(\underline{\rho})$ and $B_\Phi(\underline{\rho})$ depend only on the coordinate difference $\underline{\rho} = \underline{r}_2 - \underline{r}_1$.

The space average of a given function $A(\underline{r})$ is defined as

$$\overline{A(\underline{r})} = \lim_{\substack{X \rightarrow \infty \\ Y \rightarrow \infty}} \frac{1}{XY} \int_{-\frac{X}{2}}^{\frac{X}{2}} \int_{-\frac{Y}{2}}^{\frac{Y}{2}} A(\underline{r}) d\underline{r} \quad (5)$$

where $d\underline{r} = dx dy$. If the ensemble average $\langle A \rangle$ is equal to the space average $\overline{A(\underline{r})}$ the process is said to be ergodic. For a stationary random process $A(\underline{r})$ if the correlation function $B_A(\underline{\rho}) = \langle A(\underline{r}) A(\underline{r} + \underline{\rho}) \rangle$ is equal to the space correlation function $\overline{B_A(\underline{\rho})} = \overline{A(\underline{r}) A(\underline{r} + \underline{\rho})}$ the process is said to be ergodic with respect to its correlation function. The optical methods for measuring the correlation function generally measure the space correlation function. An important consideration as will be illustrated below is that the detail of the photomicrograph be fine enough so that a space average over the entire photomicrograph is a good approximation to the ensemble average.

An optical system can be used to produce the Fourier transform of a given photomicrograph. Thus if $g(\underline{r})$ is the complex transmittance of a particular photomicrograph whose total area is XY then the complex light amplitude in the transform plane will be proportional to the Fourier transform of $g(x,y)$ denoted by $G_{XY}(\underline{f})$ where f_x and f_y are the spatial frequencies in the x and y directions. The light intensity in the transform plane will be proportional to $|G_{XY}(\underline{f})|^2 = G_{XY}(\underline{f})G_{XY}^*(\underline{f})$ where \underline{f} is used to denote the spatial frequency vector $\underline{f} = f_x \underline{u}_x + f_y \underline{u}_y$.

For the complex random signal $g(\underline{r})$ (assumed to be stationary) the autocorrelation function $B_g(\underline{\rho})$ is defined as

$$B_g(\underline{\rho}) = \langle g(\underline{r}) g^*(\underline{r} + \underline{\rho}) \rangle \quad (6)$$

The power spectral density $S_g(\underline{f})$ of the random process $g(\underline{r})$ is defined as the two-dimensional Fourier transform of the autocorrelation function $B_g(\underline{\rho})$. Thus

$$S_g(\underline{f}) = \int_{-\infty}^{\infty} B_g(\underline{\rho}) e^{-j2\pi \underline{f} \cdot \underline{\rho}} d\underline{\rho} \quad (7)$$

One can show that $S(\underline{f})$ is also related to the Fourier transform of $g(\underline{r})$ by the expression

$$S_g(\underline{f}) = \lim_{\substack{X \rightarrow \infty \\ Y \rightarrow \infty}} \left\langle \frac{1}{XY} G_{XY}(\underline{f}) G_{XY}^*(\underline{f}) \right\rangle \quad (8)$$

In the case of the optical experiment $S_g(\underline{f})$ is seen to be proportional to the limit of an ensemble average of the intensity measured in the transform plane. This effect will be shown in some experimental results discussed below.

The autocorrelation function $B_{\tilde{g}}(\rho)$ is given from (7) by the inverse relation

$$B_{\tilde{g}}(\rho) = \int_{-\infty}^{\infty} S_{\tilde{g}}(\tilde{f}) e^{j2\pi\tilde{f}\cdot\rho} d\tilde{f} \quad (9)$$

$S_{\tilde{g}}(\tilde{f})$ can be recorded on photographic film in the transform plane of $\tilde{g}(\tilde{r})$. This new signal can then be transformed optically to give the autocorrelation function according to (9). Examples of this type of measurement will be described below.

Often the photomicrograph will be characterized by only its amplitude transmittance $A(\tilde{r})$ or by only its phase transmittance $\phi(\tilde{r})$. In general it will be necessary to relate the statistical properties of $A(\tilde{r})$ and $\phi(\tilde{r})$ to the measured statistical properties of $\tilde{g}(\tilde{r})$. Some progress along these lines has been made and efforts in this area will continue with emphasis placed on being able to experimentally measure these statistical properties

III. Power Spectrum and Autocorrelation Measurements

A schematic of the basic system used for optical processing is shown in Figure 2. A collimated beam of coherent light is incident from the left on a photomicrograph $g(x,y)$ that is inserted in the input plane. The distribution of diffracted light that appears in the transform plane is proportional to the two-dimensional Fourier transform $G_{XY}(f_x, f_y)$. A photographic film in the transform plane will record the light intensity which is proportional to $|G_{XY}(f)|^2 = G_{XY}(f)G_{XY}^*(f)$. If a filter consisting of some type of mask is placed in the transform plane then the filtered image of the original photomicrograph will appear in the output plane.

As a simple example of a random diffracting screen let the signal in the input plane be two circular holes of diameter a separated by a distance d with the line of centers oriented at an angle θ to the x -axis as shown in Figure 3. Let θ be a random variable with a uniform probability density. A circular aperture centered at the origin can be denoted by

$$g_o(r) = \text{circ} \left(\frac{r}{a/2} \right) \quad (10)$$

where $\text{circ}(r) = 1$ for $r \leq 1$ and is equal to zero otherwise. The Fourier transform of $g_o(r)$ is

$$G_o(f) = \left(\frac{a}{2} \right)^2 \frac{J_1(\pi a f_o)}{a f_o / 2} \quad (11)$$

where $f_o = \sqrt{f_x^2 + f_y^2}$ and J_1 is a Bessel function of the first kind, order one. The two hole signal in Figure 3 can then be written as

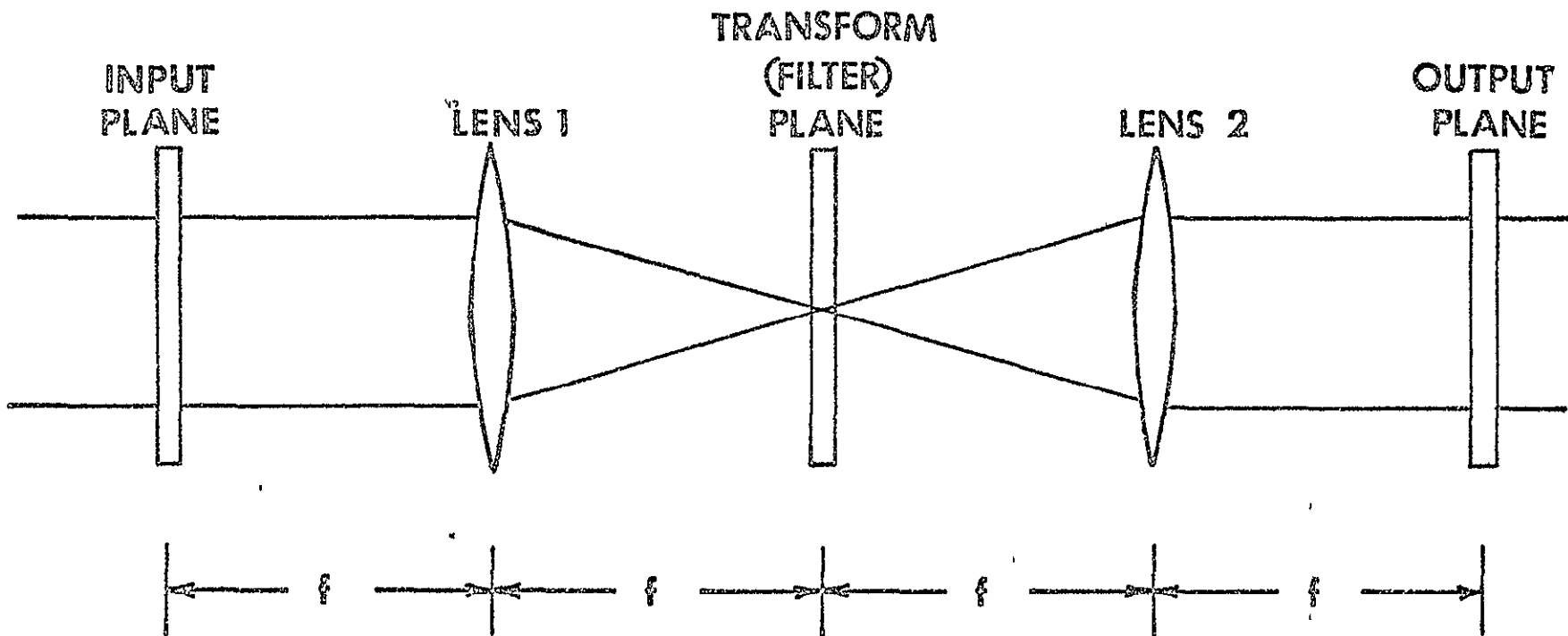


Fig. 2
Optical Processing System

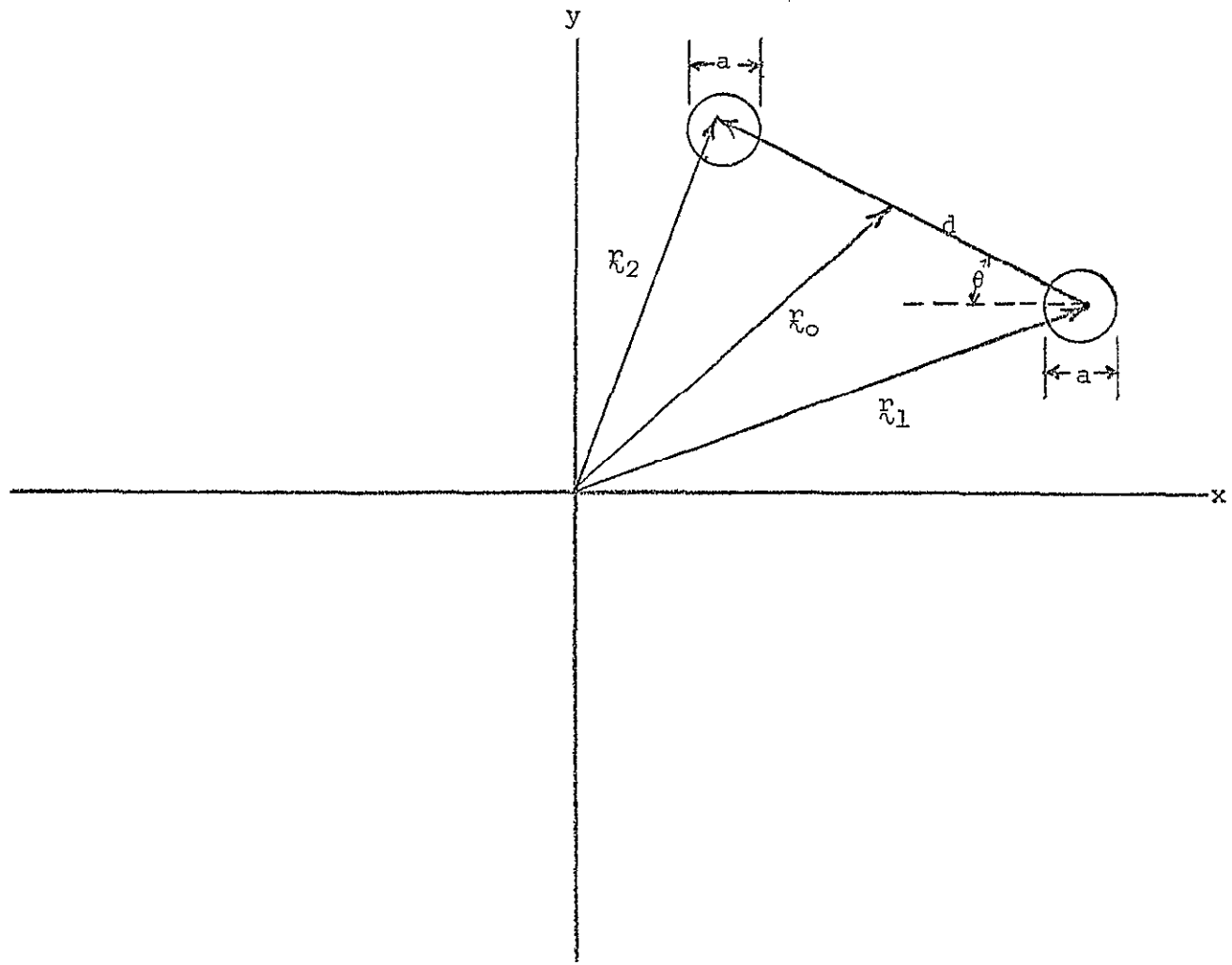


Fig 3
Geometry of Two-hole Pattern

$$g(r_{\nu}) = g_o(r_{\nu}) \cdot [\delta(r_{\nu} - r_{\nu 1}) + \delta(r_{\nu} - r_{\nu 2})] \quad (12)$$

The Fourier transform of (12) is

$$G(f_{\nu}) = G_o(f_{\nu}) [e^{-j2\pi f_{\nu} \cdot r_{\nu 1}} + e^{-j2\pi f_{\nu} \cdot r_{\nu 2}}] \quad (13)$$

Making the substitutions $r_{\nu 1} = r_{\nu o} - \frac{1}{2} d_{\nu}$ and $r_{\nu 2} = r_{\nu o} + \frac{1}{2} d_{\nu}$ Eq. (13) can be written in the form

$$G(f_{\nu}) = e^{-j2\pi f_{\nu} \cdot r_{\nu o}} 2 G_o(f_{\nu}) \cos \pi f_{\nu} \cdot d_{\nu} \quad (14)$$

The intensity in the transform plane will then be proportional to $G(f_{\nu})G^*(f_{\nu})$ where

$$G(f_{\nu})G^*(f_{\nu}) = 2 G_o^2(f_{\nu}) [1 + \cos 2\pi f_{\nu} \cdot d_{\nu}] \quad (15)$$

Figures 4 and 5 show a two hole pattern and its transform pattern which closely follows Eq (15). The fact that the envelope in Fig 5 is not circularly symmetric as predicted by (11) is due to the fact that the two holes (produced by punching holes in aluminum foil) are not perfectly circular. However, the cosine modulation of the envelope which is related to the separation distance d is clearly visible

To obtain the power spectrum of the random process an ensemble average over all orientations of the two hole signal is required

From (15) one can calculate

$$\begin{aligned} G(f_{\nu})G^*(f_{\nu}) &= 2 G_o^2(f_{\nu}) + 2 G_o^2(f_{\nu}) \int_0^{2\pi} \frac{1}{2\pi} \cos[2\pi f_o d \cos(\theta - \psi)] d\theta \\ &= 2 G_o^2(f_{\nu}) [1 + J_0(2\pi f_o d)] \end{aligned} \quad (16)$$

Fig. 4
Two-hole Pattern

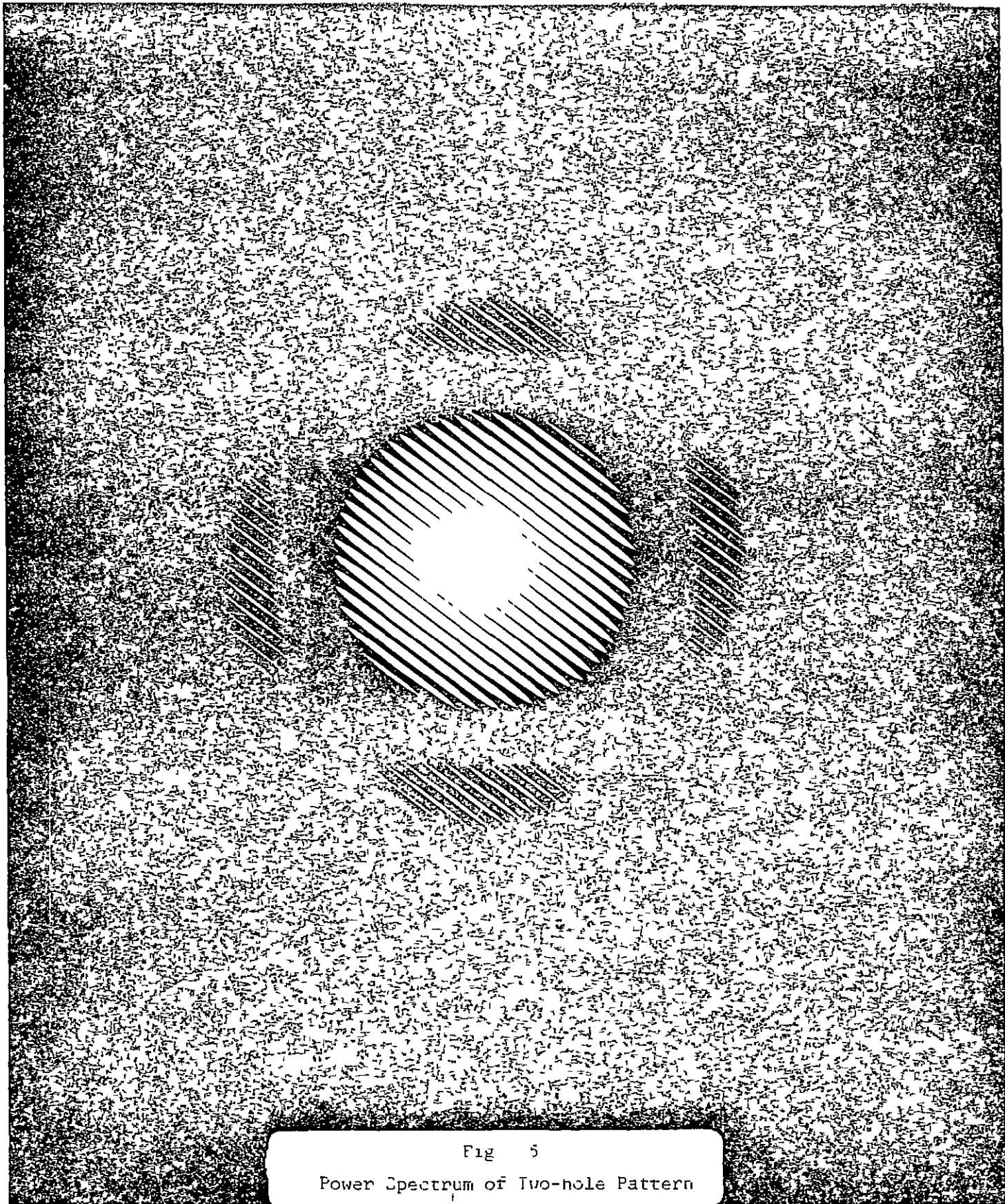


Fig 5

Power Spectrum of Two-hole Pattern

where $f_y \cdot d = f_0 d \cos(\theta - \psi)$ has been used and $\psi = \tan^{-1}(f_y/f_x)$. From (16) one notes that the power spectrum is proportional to the single hole transform given by (11) which is modulated by a J_0 Bessel function term that contains information about the separation distance d . As an attempt to measure an ensemble average a multiple exposure of the transform plane for a large number of different orientations θ is shown in Figure 6. Techniques for improving this type of measurement and scanning the resulting intensity to detect the modulations are under investigation.

In the photomicrograph problem one would like to have the random sample of large enough extent so that the transform of a single photomicrograph will determine the power spectrum of the ensemble (ergodic hypothesis). For example, Figures 7 and 8 are photomicrographs of different regions of a rabbit lens epithelium. The power spectrum of these two photomicrographs are shown in Figures 9 and 10. The extent to which they represent the power spectrum of a random process is being studied. Models of the lens epithelium from which power spectra can be calculated are being investigated. A lower magnification and therefore a larger number of cells in a given signal would improve the power spectrum measurements. However, this increases the chances of the signal being non-stationary since the cell distribution can change over a large region. In fact this change in distribution is an important feature in the description of cell growth and its quantitative detection by optical techniques would be an important measurement. Investigation into these areas is continuing.

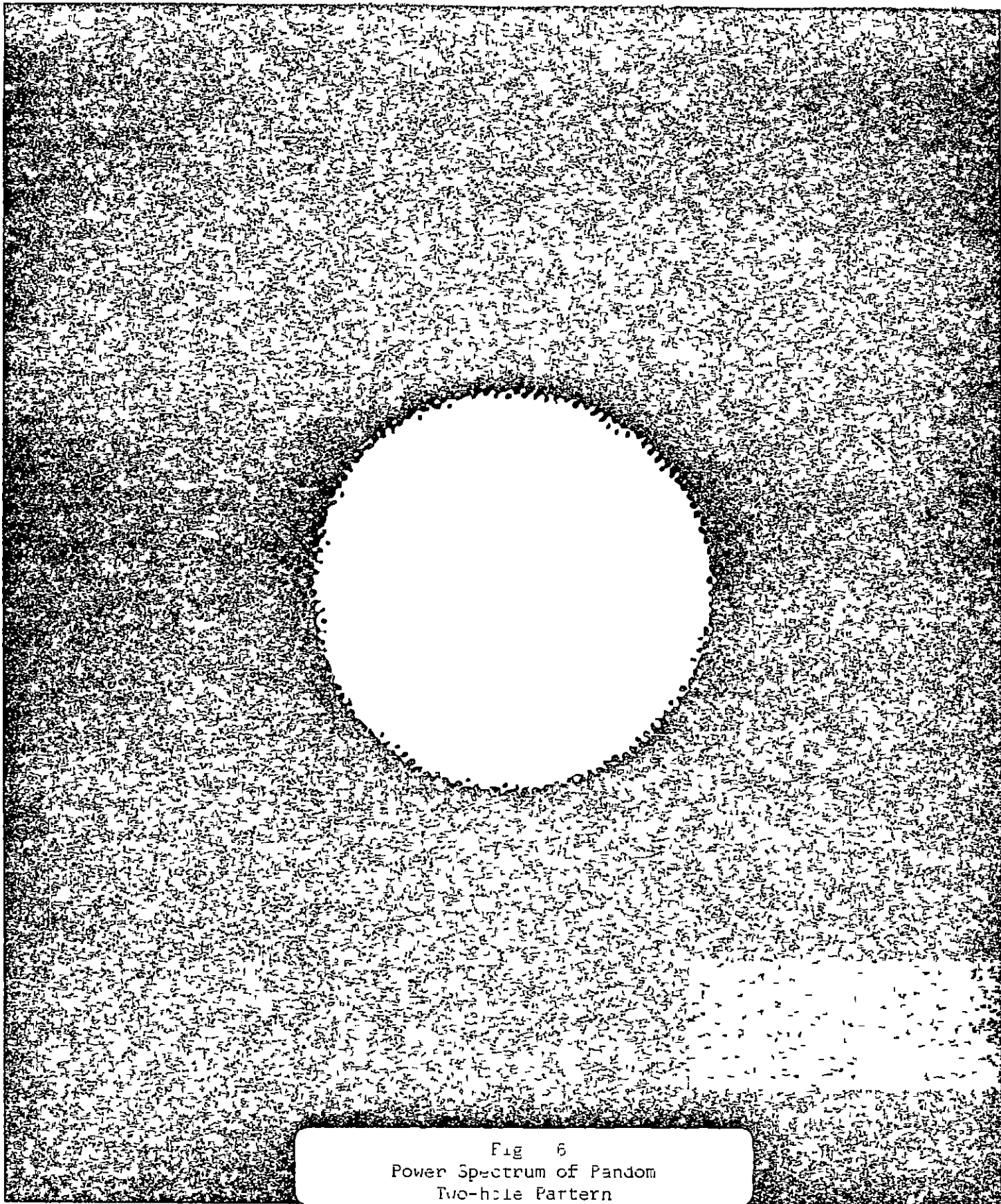


Fig 6
Power Spectrum of Pandom
Two-hole Pattern

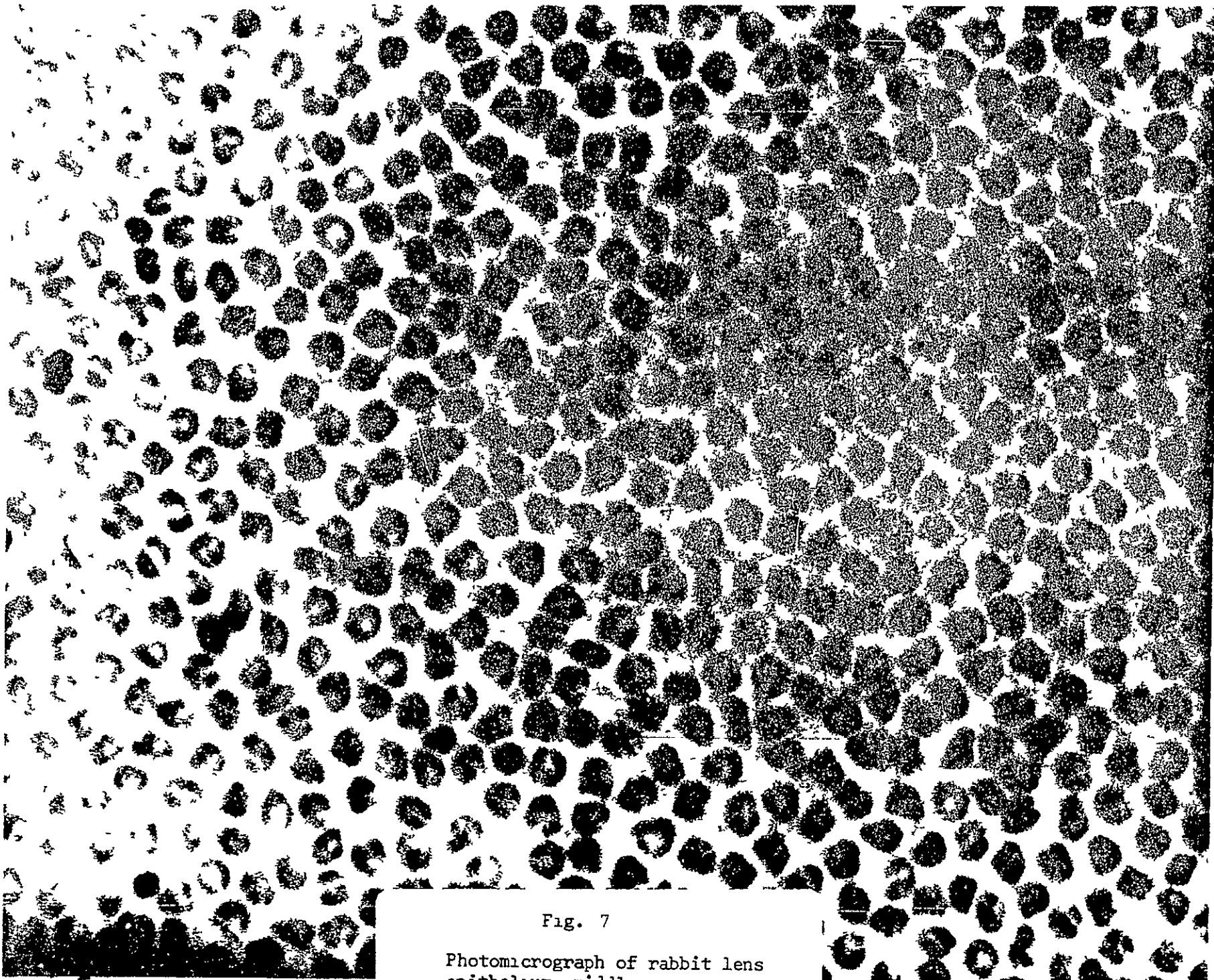


Fig. 7

Photomicrograph of rabbit lens
epithelium, middle region

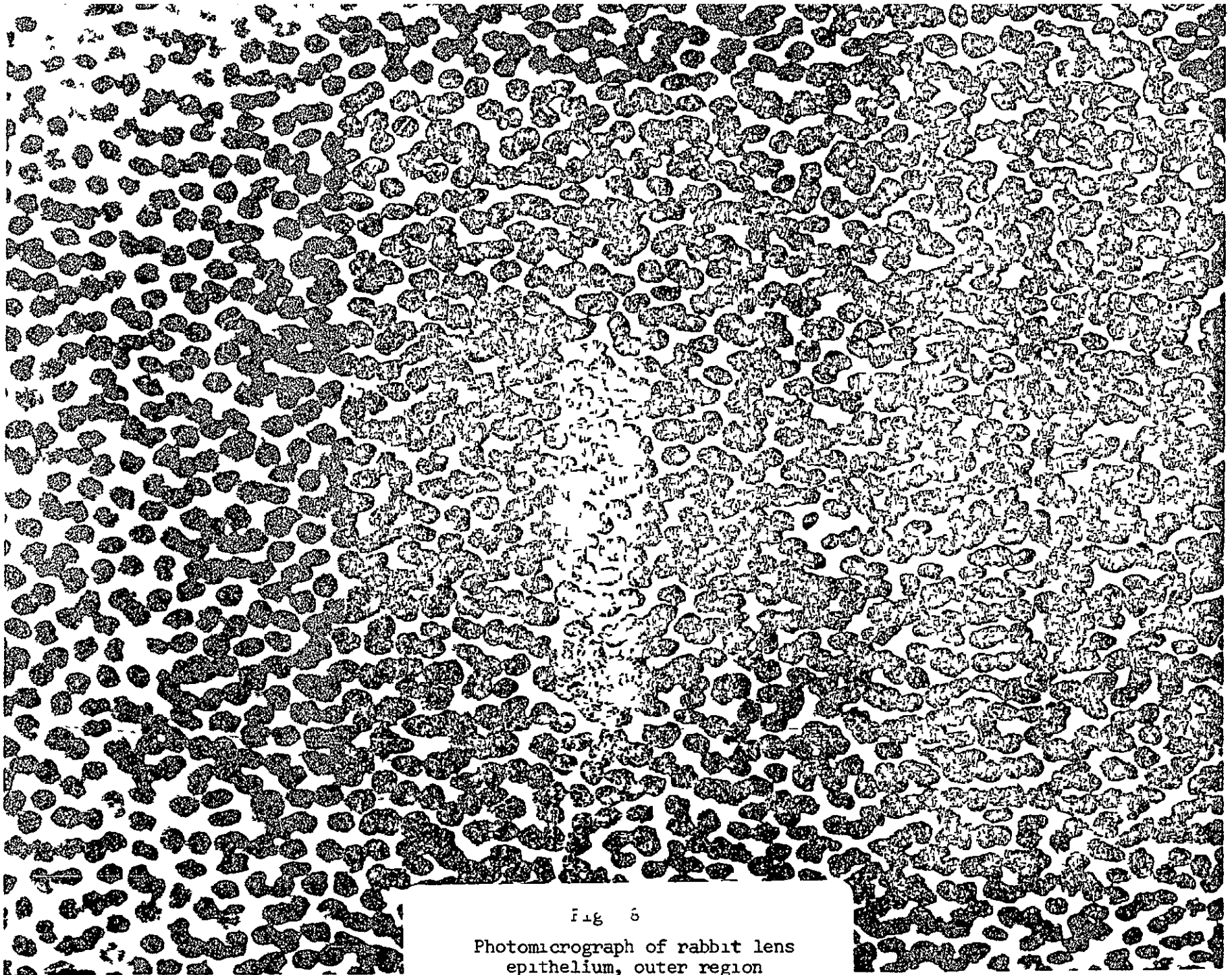


Fig 6

Photomicrograph of rabbit lens
epithelium, outer region

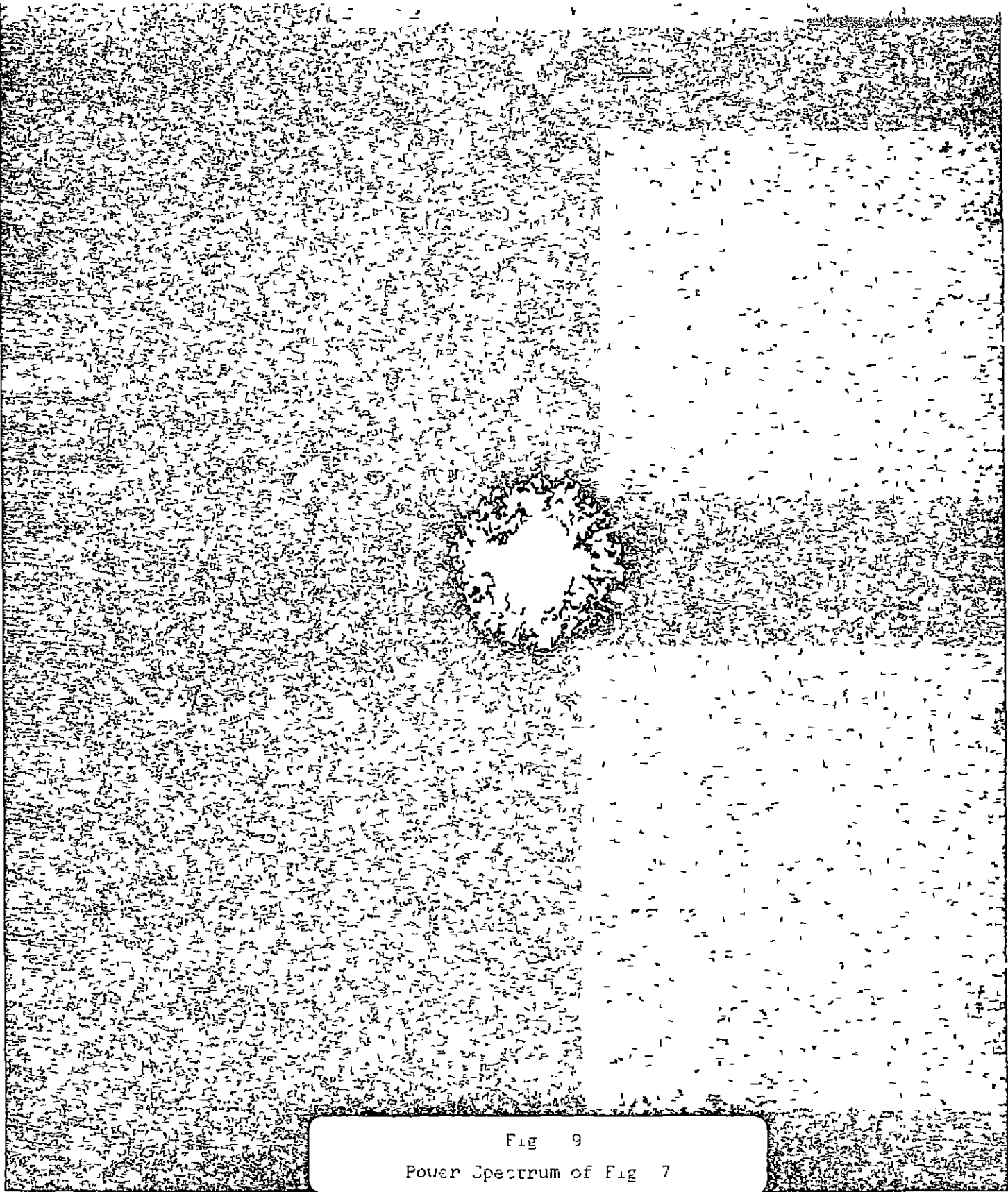


Fig 9
Power Spectrum of Fig 7

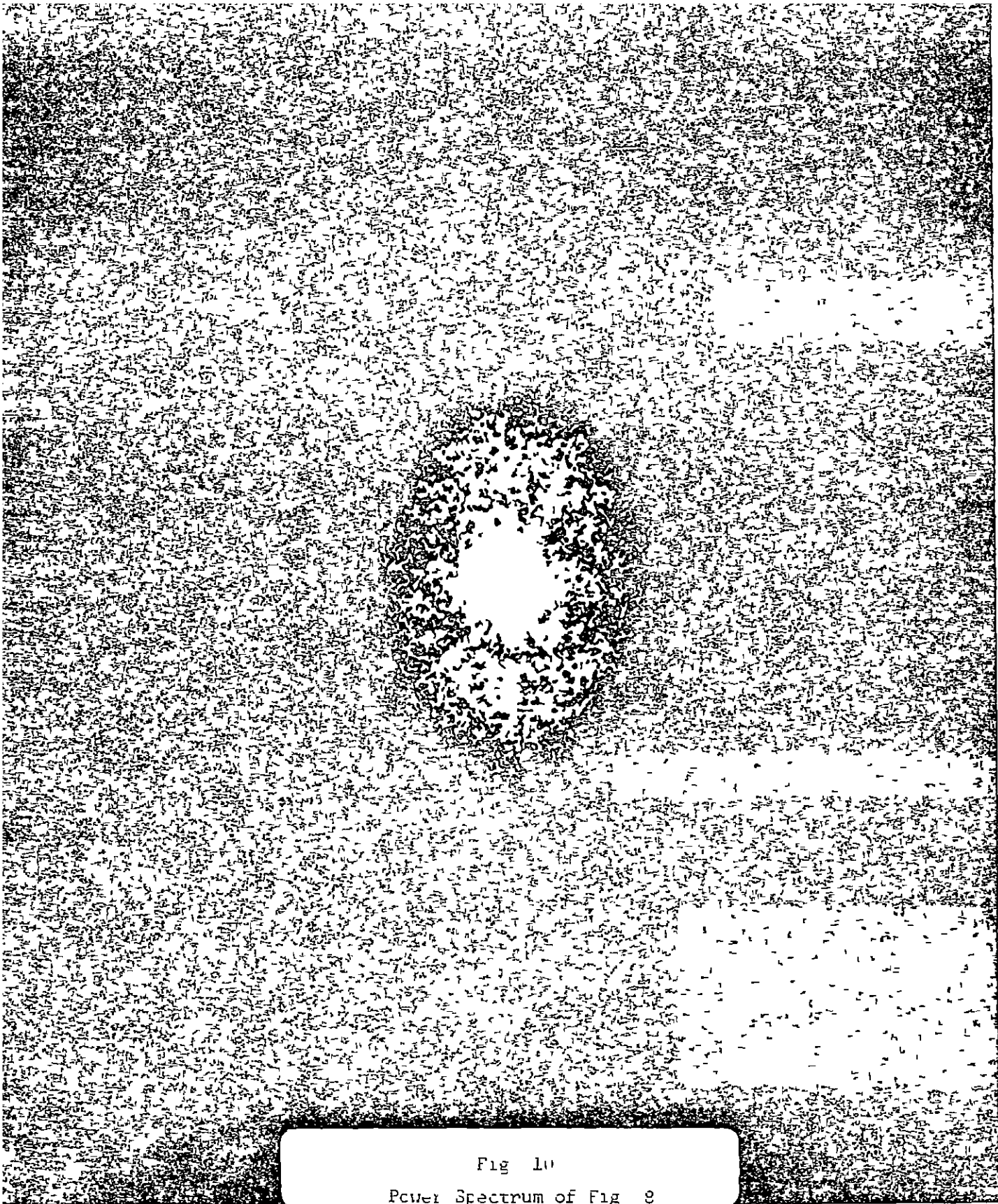


Fig 10
Power Spectrum of Fig 9

If the power spectra in Figures 9 and 10 are used as signals and their Fourier transforms are measured then one obtains the autocorrelation function according to (9). These measurements are shown in Figures 11 and 12. Again these measurements are more characteristic of the particular sample rather than the random process due to the relatively small number of cells in the sample.

IV A Lensless Optical Processor

As has been pointed out above a signal of large spatial extent is necessary if spatial averages are to replace ensemble averages. The size of spatial signals in optical processors is limited by the size of the optical components used -- particularly the size of lenses. A new optical processor that uses no lenses at all following the input pinhole has been designed and tested. The system uses a single spherical mirror as shown in Figure 13. Since high quality spherical mirrors with diameters of 8 or 10 inches are not uncommon a larger input plane format is possible with this type of processor than with the standard types using lenses. A detailed analysis of this lensless processor is contained in a forthcoming paper.

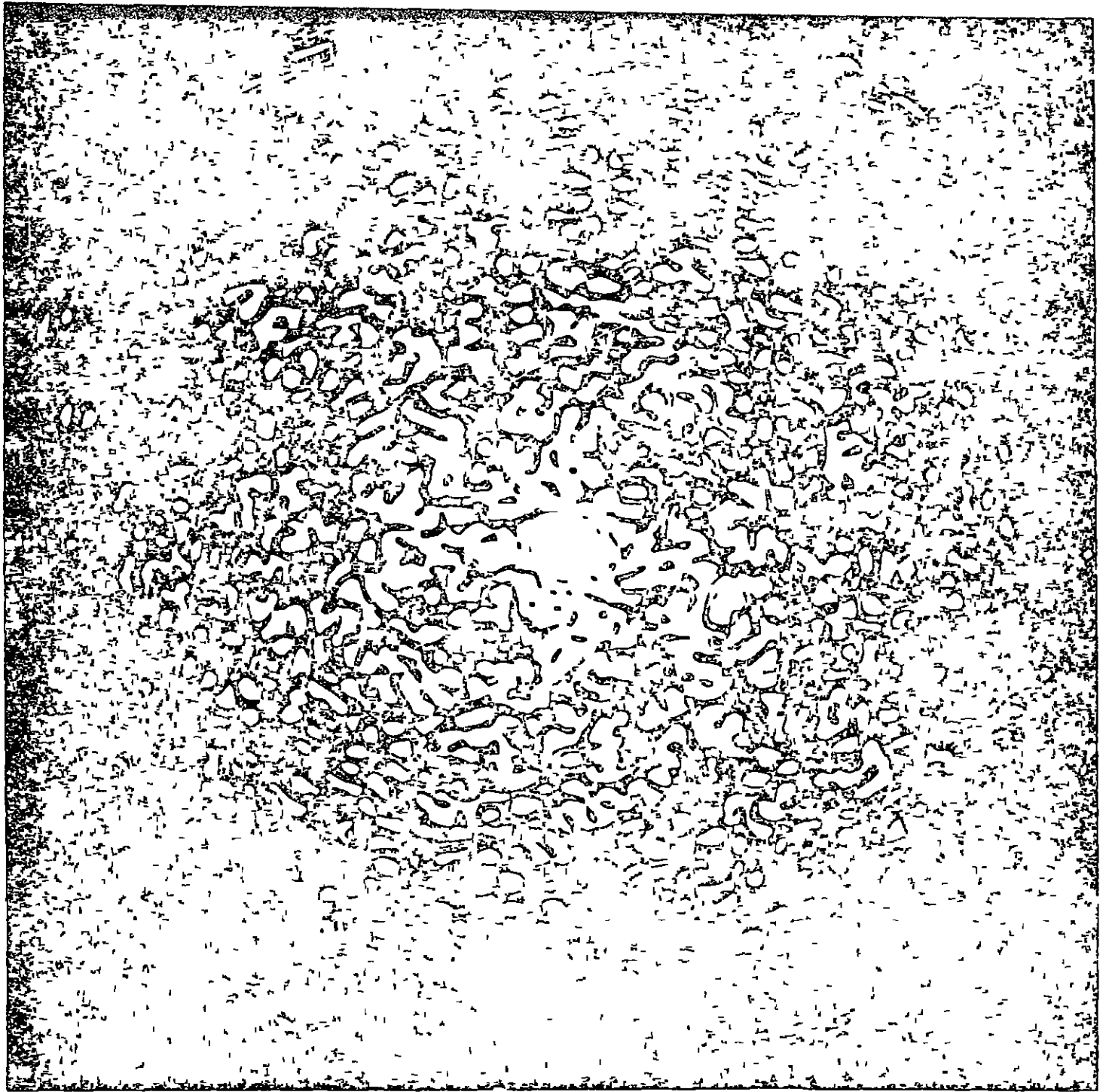


Fig 11

Autocorrelation of Fig 7

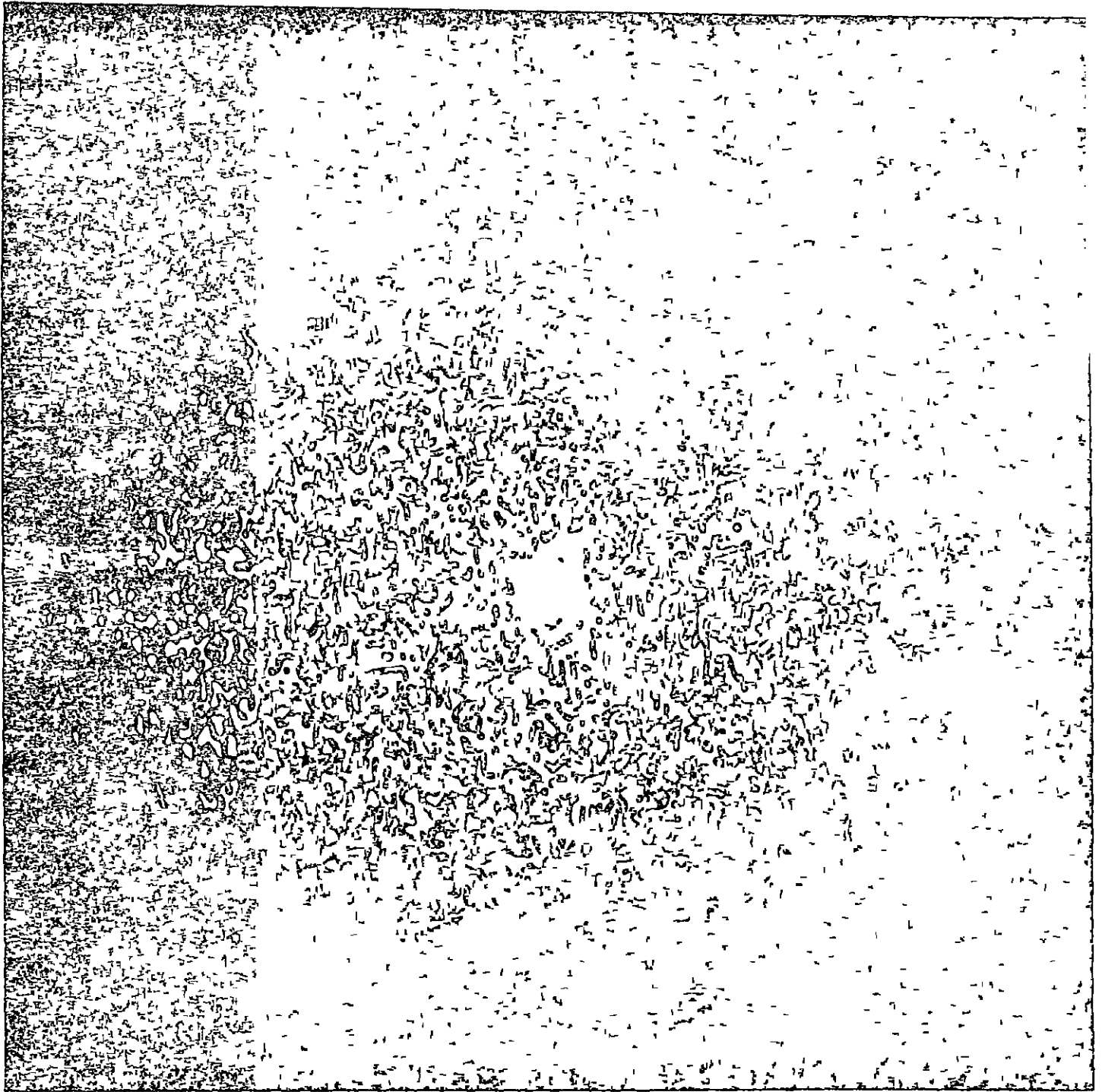


Fig. 12

Autocorrelation of Fig. 8

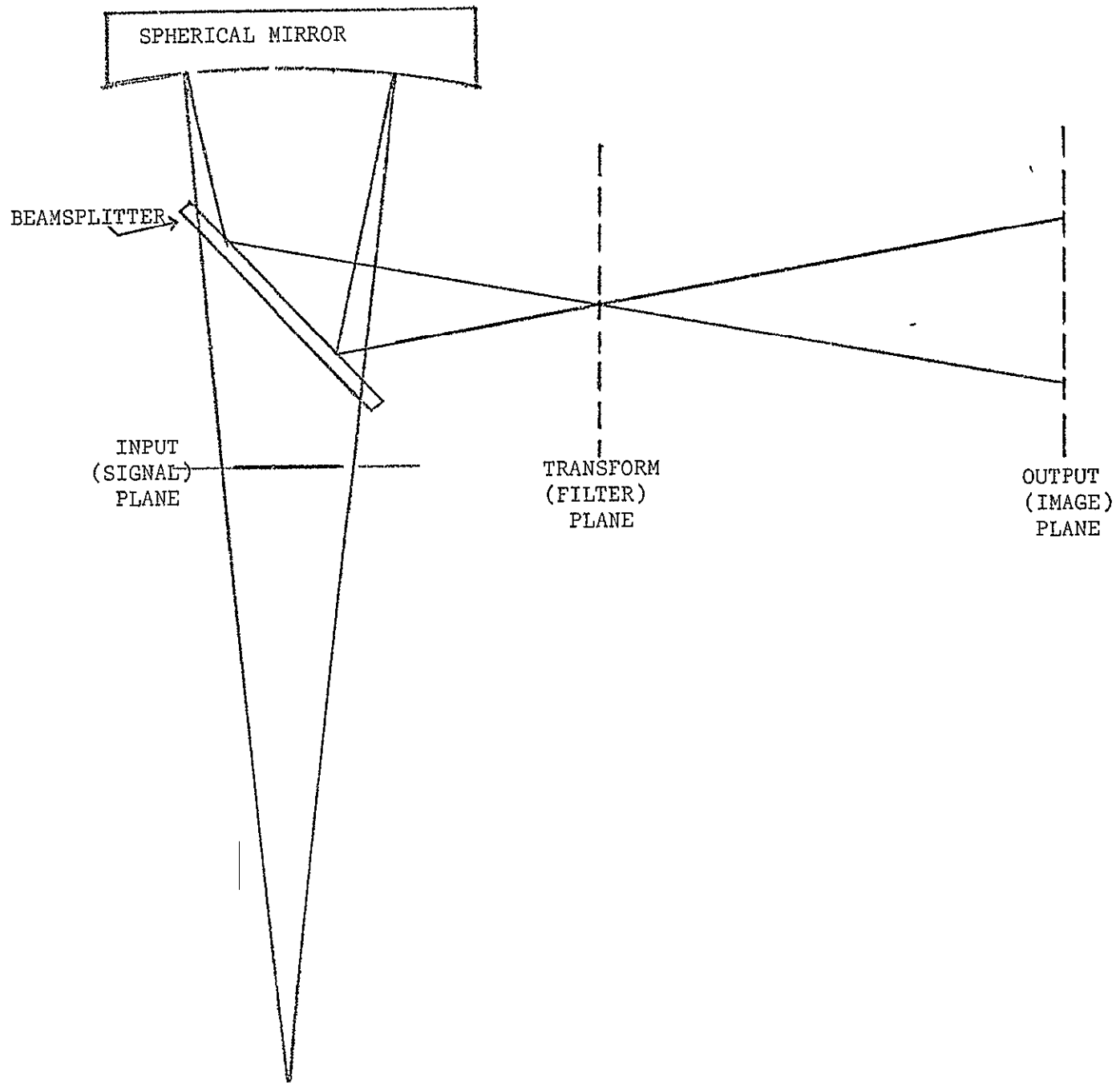


Fig. 13
Lensless Optical Processor